

1 **Short senolytic or senostatic interventions rescue progression of radiation-induced frailty and**
2 **premature ageing in mice**

3

4 **Rescue of radiation-induced premature frailty**

5

6 **Edward Fielder*, Tengfei Wan*, Ghazaleh Alimohammadiha, Abbas Ishaq¹, Evon Low, B. Melanie**
7 **Weigand², George Kelly, Craig Parker, Brigid Griffin, Diana Jurk², Viktor I. Korolchuk, Thomas von**
8 **Zglinicki#, Satomi Miwa#**

9

10 ***shared first authors**

11 **#shared last authors**

12

13 **Affiliations:**

14 Newcastle University Biosciences Institute, Newcastle University, Newcastle upon Tyne, NE4 5PL, UK

15 ¹present address: Alcyomics Ltd, The Biosphere, Newcastle Helix, Drayman's Way. NE4 5BX.

16 ²present address: Robert and Arlene Kogod Center on Aging, Department of Physiology and
17 Biomedical Engineering, Mayo Clinic, 200 First Street SW, Rochester, MN 55905, USA

18

19 **Abstract:**

20 Cancer survivors suffer from progressive frailty, multimorbidity and premature morbidity. We
21 hypothesize that therapy-induced senescence and senescence progression via bystander effects is a
22 significant cause of this premature ageing phenotype. Accordingly, the study addresses the question
23 whether a short anti-senescence intervention is able to block progression of radiation-induced frailty
24 and disability in a pre-clinical setting.

25 Male mice were sub-lethally irradiated at 5 months of age and treated (or not) with either a
26 senolytic drug (Navitoclax or dasatinib + quercetin) for 10 days or with the senostatic metformin for
27 10 weeks. Follow up was for one year. Treatments commencing within a month after irradiation
28 effectively reduced frailty progression ($p<0.05$) and improved muscle ($p<0.01$) and liver ($p<0.05$)
29 function as well as short-term memory ($p<0.05$) until advanced age with no need for repeated
30 interventions. Senolytic interventions that started late, after radiation-induced premature frailty was
31 manifest, still had beneficial effects on frailty ($p<0.05$) and short-term memory ($p<0.05$). Metformin
32 was similarly effective as senolytics. At therapeutically achievable concentrations metformin acted
33 as a senostatic neither via inhibition of mitochondrial complex I, nor via improvement of mitophagy
34 or mitochondrial function, but by reducing non-mitochondrial ROS production via NOX4 inhibition in
35 senescent cells.

36 Our study suggests that the progression of adverse long-term health and quality-of-life effects of
37 radiation exposure, as experienced by cancer survivors, might be rescued by short-term adjuvant
38 anti-senescence interventions.

39

40

41

42 **Introduction**

43 Cancer has become an increasingly survivable disease, with cancer-specific mortality in developed
44 countries having dropped sharply in the last few decades. Many cancer types have now high cure
45 rates (Bray et al., 2018), and in some fields the emphasis has started to shift towards efforts to
46 improve the quality of survivorship after successful cancer treatment (Damlaj, El Fakih, & Hashmi,
47 2019). This is necessary as long-term survivors of childhood and adult cancers undergo a wide-range
48 of negative health and quality of life changes that lead to increased frailty, multi-morbidity and
49 mortality compared to the general population (Bluethmann, Mariotto, & Rowland, 2016; Cupit-Link
50 et al., 2017; Robison & Hudson, 2014). These changes are indicative of accelerated or premature
51 ageing in long-term cancer survivors, for which there is currently no validated therapy.

52 Premature ageing in cancer survivors appears to be largely caused by DNA-damaging cancer
53 therapies. Numerous biological processes have been proposed as drivers of this (Cupit-Link et al.,
54 2017; Ness et al., 2018), with therapy-induced cell senescence prominent amongst them (Short,
55 Fielder, Miwa, & von Zglinicki, 2019).

56 Cell senescence is a complex cellular stress response program that can be induced by DNA damage
57 (e.g. radio- or chemotherapy) and involves persistent cell cycle arrest, aberrant regulation of
58 metabolism (specifically energy metabolism), epigenetic programming and secretory processes
59 (Gorgoulis et al., 2019; von Zglinicki, 2021). Therapy-induced senescence may constitute a
60 cytostatic clinical response contributing to stable disease (te Poele, Okorokov, Jardine, Cummings, &
61 Joel, 2002), however, there is increasing evidence that therapy-induced senescent cells can promote
62 both primary relapse and secondary cancers, often leading to less successful treatment outcomes of
63 consequent disease (Jena, Das, Bharadwaj, & Mandal, 2020; Saleh, Tyutyunyk-Massey, & Gewirtz,
64 2019). Senescent cells release both pro-inflammatory and pro-oxidant signaling molecules (the
65 Senescence-Associated Secretory Phenotype, SASP) which can damage and induce senescence in
66 bystander cells (Nelson et al., 2012), and thus spread the phenotype from the point of origin
67 throughout tissues and organisms (da Silva et al., 2019; Xu et al., 2018). As such, adjuvant tumour
68 therapy not only induces transiently (and locally) high concentrations of senescent cells but may also
69 result in faster accumulation of these cells both locally and systemically over the whole life course
70 (Short et al., 2019).

71 Accumulation of senescent cells is causal for a wide range of ageing-associated diseases and
72 disabilities as evidenced by the far-reaching successes of interventions that reduce the systemic load
73 of senescence [for review see (Short et al., 2019)]. In fact, acute ablation of senescent cells by
74 continuous pharmacogenetic or pharmacologic intervention has been able to reduce chemotherapy-
75 induced multimorbidity (Demaria et al., 2017) and liver toxicity (Baar et al., 2017) as well as
76 radiation-induced haemotoxicity (Chang et al., 2016) and sarcopenia (Zhu et al., 2015) in mice.
77 However, if induction of secondary senescence by bystander effects is a major driver of post-
78 therapeutic senescence, continuous anti-senescence interventions might not be necessary. Rather,
79 we hypothesized that specific ablation of senescent cells (senolytic intervention) or specific
80 inhibition of the SASP (senostatic intervention) shortly after adjuvant cancer therapy might be
81 sufficient to rescue enhanced mortality, multimorbidity and frailty in cancer survivors over their life
82 course (Short et al., 2019).

83 Senolytics are potent drugs with frequently serious side effects (Demaria, 2017) that would raise
84 significant safety concerns in a preventive setting, even in a high-risk group like tumour survivors. In
85 contrast, senostatics (sometimes also termed senomorphics) are chemicals that do not kill
86 (senescent) cells but block SASP signals, thus inhibiting the spread of senescence via bystander

87 effects. In fact, senostatic interventions, including the dietary restriction mimetics rapamycin and
88 metformin, or dietary restriction itself, caused lasting reductions of senescent cell burden in
89 different tissues of mice with improved lifespan and healthspan (Blagosklonny, 2017; Fontana,
90 Nehme, & Demaria, 2018; Lopez-Otin, Galluzzi, Freije, Madeo, & Kroemer, 2016; Selvarani,
91 Mohammed, & Richardson, 2021). However, their efficiency to rescue premature ageing has not
92 been pre-clinically tested in comparison to senolytic intervention.

93 The senostatic metformin has an extraordinarily good safety profile, which has been testified in its
94 long clinical history as well as in a myriad of clinical trials. However, the drug acts through multiple
95 pathways, and it is not at all clear how it reduces the SASP in a therapeutically achievable setting. It
96 is often assumed that it blocks complex I of the electron transport chain, thus reducing production of
97 reactive oxygen species in mitochondria, which in turn would reduce NF- κ B activation and thus the
98 SASP (Moiseeva et al., 2013). However, metformin efficiently blocks complex I only in millimolar
99 concentrations, while tissue concentrations that can be achieved in mice or man are one to two
100 orders of magnitude lower (Wilcock & Bailey, 1994). A mechanistic examination of the senostatic
101 effect of metformin *in vivo* is therefore urgently warranted.

102 To address these questions in a pre-clinical setting, we used a simple mouse model of premature
103 ageing induced by fractionated whole-body irradiation (Fielder et al., 2019). We show here that i)
104 irradiation-induced lifelong premature ageing can be rescued by a one-off post-irradiation senolytic
105 intervention, ii) senolytics are still partially efficient in reducing progression after establishment of a
106 premature ageing phenotype, iii) a relatively short metformin intervention is similarly effective in
107 rescuing premature ageing and iv) metformin at therapeutic concentrations acts as a senostatic
108 neither via inhibition of complex I, nor via improvement of mitophagy or mitochondrial function, but
109 by reducing non-mitochondrial ROS production in senescent cells.

110

111

112

113 **Materials and Methods**

114 **Study design**

115 This study addressed the hypothesis that premature frailty and accelerated ageing after sublethal
116 irradiation are caused by accelerated accumulation of senescent cells triggered by bystander
117 signalling from radiation-induced senescence, and that thus a short treatment with either a senolytic
118 or the senostatic metformin would be protective. A series of controlled laboratory experiments were
119 performed to determine the progression of frailty and other markers of biological age following
120 irradiation with and without intervention at prespecified time points. All studies were conducted at
121 Newcastle University in agreement with ARRIVE guidelines (Kilkenny, Browne, Cuthill, Emerson, &
122 Altman, 2010). On the basis of previous work, two-sided two-sample test were used to generate
123 animal group sizes. Incorporating expected attrition rates during long-term follow-up, this resulted
124 in group sizes of 12 animals at start of the experiments for physiological phenotyping. Data
125 collection was performed at prespecified time points unless limited by animal distress as identified
126 by facility staff and/or veterinary surgeons. Primary and secondary end points were prespecified.
127 Each mouse represented one experimental unit. Mice were coded with randomized allocation to
128 experimental groups and housing cages. Data collection, tissue collection and tissue analyses were
129 done by staff members blinded to experimental group allocation with unblinding performed only
130 after data acquisition was complete. For ex-vivo assessments, power calculations informed by
131 previous experience indicated a minimum number of 5 animals per group. Tissues were either
132 randomly selected or all available tissues were used for analysis.

133 To address the mechanism of senostatic activity of metformin in therapeutically achievable
134 concentration, a stepwise series of controlled laboratory *in vitro* experiments was performed, where
135 experimental outcomes guided alternative hypotheses. Individual cell culture dishes represented
136 experimental replicates except in the case of mitophagy experiments, where each cell was treated as
137 a biological unit. Again, *in vitro* treatments were coded and codes were broken only after data
138 collection and analysis. *In vitro* experiments were independently reproduced at least three times.

139 **Animals**

140 Male C57Bl/6J mice were bought past weaning from Charles River and were maintained in groups of
141 six littermates per cage as described (Cameron, Miwa, Walker, & von Zglinicki, 2012). The mice were
142 fed standard pelleted food (CRM-P formulation rodent diet, SDS Diets), except those used for
143 metformin treatment and their control, which received soaked food (same as above) with or without
144 metformin from one-month post-IR. Mice were sacrificed at the end of the study by cervical
145 dislocation and tissues harvested, and stored in 4% paraformaldehyde for 24 hours for paraffin
146 embedding, or frozen in liquid nitrogen. The work was licensed by the UK Home Office (PB048F3A0)
147 and complied with the guiding principles for the care and use of laboratory animals.

148 **Irradiation**

149 At 5 months of age, mice were sub-lethally irradiated thrice (NDT320, 225kV) with 3 Gy of X-ray
150 irradiation, with two days of recovery between each dose, as described (Fielder et al., 2019). Mice
151 received 1% Baytril solution in drinking water for 2 days before, and for 14 days after, to the start
152 and end of irradiation, respectively.

153 **Senolytic and senostatic treatments**

154 Mice were orally gavaged with either 5mg/kg/day dasatinib and 50mg/kg/day quercetin or with
155 5mg/kg/day Navitoclax for 10 days total (5 days, 2 days recovery, and 5 days). Compounds were

156 prepared for oral gavage in 10% Polyethylene Glycol (PEG400). Control mice were gavaged with
157 PEG400 only. Interventions were started at 1 month post-irradiation for the early intervention
158 group, and 7 months post-irradiation for the late intervention group. Dasatinib (CDS023389),
159 quercetin (1592409), and PEG400 (8074851000) were purchased from Sigma-Aldrich (now Merck).
160 Navitoclax (285063-USB) was purchased from Stratech.

161 Metformin hydrochloride was a kind gift from FARMHISPANIA, (Barcelona) and prepared at 1g/kg in
162 dry food (0.1% (w/w) in food) and provided at 6mg/6ml water in 6g food per mouse in the cage.
163 Treatment was started at 1 month post-irradiation and was given daily for 10 weeks.

164 **Mouse phenotyping**

165 Frailty was assessed regularly using a 30-parameter index based on (Whitehead et al., 2014), with
166 modifications as described in (Fielder et al., 2019). Rotarod, wire hanging and spontaneous
167 alternation Y-Maze were performed as described in (Fielder et al., 2019). Tumour incidence at death
168 was assessed by gross pathological examination.

169 **Immuno-histochemistry (IHC) and immunofluorescence**

170 Paraformaldehyde (PFA)-fixed paraffin embedded tissue samples were cut and stained with primary
171 and secondary antibodies as detailed in Table 1, see also (Fielder et al., 2020) for a step-by-step
172 protocol. Fixed cells were blocked with 2% normal goat serum + 0.1% BSA and stained overnight
173 with the primary antibody at 4C (Tab 1).

174 **Immuno-fluorescence in situ hybridisation (immuno-FISH)**

175 The Immuno-FISH for telomere associated foci (TAF) were performed as previously described
176 (Hewitt et al., 2012), (Fielder et al., 2020) with the following modifications for quadriceps: The
177 blocking step used 1% BSA, 5% Normal Goat Serum in PBS, for 30 minutes at 30°C. Fluorescein Avidin
178 DCS was substituted with Texas Red-labelled Avidin DCS (Vector Laboratories) in PBS for 30 minutes
179 at 30°C. CCCTAA Cy-3 probe was substituted for TTAGGG probe (Pangene).

180 **Microscopy and image analysis**

181 IHC images were taken using a widefield light microscope ECLIPSE E800 (Nikon, Japan) at total
182 magnification of 100x. Microscopy for IF and immuno-FISH was performed using a DMI8
183 fluorescence microscope (Leica, Germany) with total magnification of 400x for IF and 630x (with Z-
184 stack/depth) for immuno-FISH.

185 Positive and negative nuclei were manually identified by observers blinded to the treatment groups,
186 counted on 5 images per animal and the average was calculated as the individual value for the
187 sample/animal. Nuclear size was manually measured with ImageJ software (NIH, USA).

188 Epidermal thickness was measured on 3 μm back skin sections stained with Picro-sirius red/fast
189 green. 3 different regions were imaged per animal, and 25 measurements were taken in each region
190 using the straight-line tool in ImageJ.

191 To identify TAF in brain, the colocalisation of DNA damage foci and telomeres were detected
192 manually and confirmed in Icy software through 3D image setup as described (Hewitt et al., 2012),
193 (Fielder et al., 2020). For liver and muscle, detection and 3D location of DNA damage foci and
194 telomeres was automated using Icy software (Institut Pasteur & France Bioimaging, France). A
195 Python programme was used to assess their colocalization. Results from this automated counting
196 were validated against manual counts in individual liver and muscle sections.

197 **Western blotting**

198 Cells were collected using Accutase (StemCell Technologies #07922) and lysed using RIPA buffer
199 supplemented with protease inhibitors. Western blotting was performed as described (Miwa et al.,
200 2014) with antibodies against NOX4 and β -Actin as detailed in Table 1.

201 **Liver function assessment**

202 Liver function was assessed using the Alanine Transaminase Activity Assay Kit (Abcam, ab105134)
203 and Aspartate Aminotransferase Activity Assay Kit (Abcam, ab105135) according to the
204 manufacturer's instructions. Average of duplicates was used as individual data of a sample/animal,
205 and then the data were grouped by treatment types and compared.

206 **Cell culture**

207 Human lung MRC5 fibroblasts were grown in Dulbecco's modified Eagle's medium (DMEM, Sigma, #
208 D5671) supplemented with 10% heat-inactivated foetal Bovine Serum (FBS, Sigma), 100 units/ml
209 penicillin, 100 μ g/ml streptomycin and 2 mM L-glutamine at 37°C in a humidified atmosphere with
210 5% CO₂. Stress-induced senescence was induced by X-ray irradiation with 20 Gy or (for DPI
211 experiments) with 200 μ M H₂O₂ in serum-free medium.

212 For metformin treatment, medium was replaced with fresh medium containing 100 μ M metformin or
213 DMSO (vehicle control) immediately post irradiation. Treatment was maintained for 10 days, with
214 medium changes every 3 days.

215 For NOX4 overexpression, pcDNA3.1-hNOX4 (Addgene #69352) was used, with pcDNA3.1(+)eGFP
216 (Addgene #129020) as control. Plasmids were extracted using the EndoFree Plasmid Maxi Kit
217 (Qiagen 12362). 80% confluence MRC5 cells (PD 15-25) were transfected using 500ng of plasmid per
218 well with Lipofectamine 3000 (ThermoFisher L3000001). For selection, cells were grown for one
219 week in G418 (400 μ g/ml) from the 3rd day post-transfection and fixed with 4% PFA for staining.

220 For NOX4 inhibition, senescent MRC5 cells treated with diphenyleneiodonium chloride (DPI, Bio-
221 Techne 4673-26-1 at either 50nM, 10nM or DMSO control) for 3 days.

222 For Sen- β -Gal staining, cells were fixed for 5 min with 2% PFA in PBS-Mg before incubation with the
223 staining solution (PBS-Mg containing 1mg/ml X-gal, 5mM potassium ferrocyanide and 5mM
224 potassium ferricyanide, pH 5.5) overnight at 37C.

225 **Mitophagy measurement**

226 Neonatal human dermal fibroblasts (HDFns) were transduced with lentiviruses containing pCHAC-
227 mt-mKeima (Addgene plasmid #72342) (Lazarou et al., 2015). Cells were irradiated with 20Gy X-ray
228 radiation and the mt-mKeima signal was measured up to 3 days later. During this time cells were
229 treated with metformin (100 μ M) or rapamycin (10nM). The live-cell mt-mKeima signal was captured
230 on a Leica DMi8 inverted microscope with a 63x oil objective. Numbers of red dots per cell,
231 indicating lysosomal mt-mKeima signal were quantified using ImageJ.

232 **ROS measurements**

233 Cells were stained with dihydroethidium (DHE, ThermoFisher Scientific) to measure intracellular
234 peroxides or with MitoSOX (ThermoFisher Scientific) to assess mitochondrial superoxide. Cells were
235 incubated with either 10 μ M DHE or 5 μ M MitoSOX for 30 min at 37°C in the dark and analysed by
236 flow cytometry or in a DMi8 fluorescence microscope (Leica).

237 Extracellular release of hydrogen peroxide was measured by Amplex Red assay (ThermoFisher
238 Scientific) as described (Miwa et al., 2016) in a 96 well plate using a fluorescent plate reader
239 (FLUOstar Omega, BMG Labtech) at excitation 544nm and emission 590 nm at 37°C.

240 **Oxygen consumption rates**

241 Cellular oxygen consumption rates (OCR) and media acidification rates (extracellular acidification
242 rate, ECAR) in intact cells were measured in parallel using a Seahorse XF24 analyzer in unbuffered
243 basic media (DMEM, Sigma, #D5030) supplemented with 5mM glucose, 2mM L-Glutamine and 3%
244 FBS. Whilst the measurements were taken, the following compounds were injected to test
245 mitochondrial activity and cellular bioenergetics: Oligomycin (0.5µM) to inhibit ATP synthase,
246 carbonyl cyanide p-trifluoromethoxy-phenylhydrazone (FCCP) (2.5µM), a respiratory chain
247 uncoupler, 2-deoxyglucose (2DG) (80mM), a glucose analogue competitively inhibiting glucose
248 uptake and glycolytic flux, and Rotenone (0.5µM) and Antimycin (2.5µM), mitochondrial complex I
249 and complex III inhibitors, respectively. Data analysis to calculate absolute ATP production rates was
250 carried out using the methods described by Mookerjee and Brand (Mookerjee & Brand, 2015) taking
251 into account the acidification rates due to mitochondrial CO₂ production (Birket et al., 2011; Brand,
252 2005).

253 Permeabilised cells were used to measure mitochondrial oxygen consumption rates using Pyruvate
254 (10mM) and Malate (1mM) as complex I-linked substrate. Cells were permeabilised using Plasma
255 membrane permeabiliser (PMP, Agilent Technologies) according to manufacturer's instructions, and
256 oxygen consumption was measured in medium containing 220mM Mannitol, 70mM Sucrose, 10mM
257 KH₂PO₄, 5mM MgCl₂, 2mM Hepes, 1mM EGTA and 0.2% (w/v) Fatty Acid Free BSA. To determine the
258 effects of metformin on mitochondrial complex I activity, sequential additions of metformin (at
259 concentrations as indicated in Figure 4A), Rotenone (0.5µM), Succinate (4mM), and FCCP (4µM)
260 were made. For determination of Respiratory Control Ratio (RCR), permeabilised cells respiring with
261 Pyruvate (10mM) and Malate (1mM) received 4mM ATP (State 3) followed by 0.5µM Oligomycin
262 (State 4). RCR was calculated as state 3 divided by state 4 respiration rates.

263 **Cytokine measurement**

264 Cytokines secreted from MRC5 cells were analysed by Human Cytokine Array Proinflammatory
265 focused 13-plex Assay (Eve Technologies, Calgary, Canada). The cells were grown in 75cm flasks, and
266 the culture media was switched to serum free media for 24 hours and the media samples were
267 collected for the analysis.

268 **Mass Cytometry**

269 Markers for multiple stress response pathways (Table 2) were analysed at single cell level
270 simultaneously by mass cytometry (Helios, Fluidigm). MRC5 cells were treated with either 2mM or
271 0.1 mM metformin for 2 days. Positive controls were challenged with either 300 µM H₂O₂ in serum-
272 free medium, heat shock (50°C for 45 min) or starvation (serum-free medium for 24 h). The cells
273 were trypsinized, washed in PBS, and stained with metal-conjugated antibodies (Table 2). Antibodies
274 were either pre-conjugated (Fluidigm), or purified antibodies were conjugated to lanthanide metals
275 using the Maxpar antibody labeling kit (as per manufacturer's instructions; DVS Sciences) and were
276 stabilised with an antibody stabilisation solution (Candor Bioscience) (Table 2). Cells were stained as
277 described (Cytlak et al., 2020). Briefly, cells were first stained with 2.5µM Cisplatin (Fluidigm
278 #201064) for 5 minutes in PBS for live/dead cell discrimination and washed promptly using Wash
279 buffer (PBS containing 2% FBS). Then the cells were fixed using 1.6% formaldehyde in a working
280 fixation buffer (eBioscience Foxp 3 fixation permeabilisation kit, ThermoFisher Scintific #00-5523) for

281 30 minutes, and washed twice with eBioscience perm buffer. Cells were stained in perm buffer for
282 1hr with the antibody cocktail containing each intracellular antibody (approximately 0.5 μ g in 100 μ L
283 per sample) for 1 hour at room temperature and washed twice with PBS. Finally the cells were fixed
284 with 1.6% formaldehyde in PBS with a nuclear marker, 125nM iridium (Cell-ID™ Intercalator-Ir,
285 Fluidigm #201192B) for 1 hour, and washed using Wash buffer for overnight storage at 4°C. Prior to
286 CyTOF acquisition, cells were washed twice in 200 μ L MilliQ water (600xg for 5 minutes), counted,
287 diluted to a maximum final concentration of 0.55 \times 10 6 /ml in MilliQ water and filtered through a 40
288 μ m filter (BD). EQ beads were added (10% by volume) and 0.1 \times 10 6 cells per sample were acquired on
289 the Helios mass cytometer running CyTOF software v 6.7.1014. The data were analysed using FCS
290 Express 7 (De Novo Software).

291 **Statistics**

292 Data were analysed with Microsoft Excel and Prism software (GraphPad). Values were expressed
293 either as means with error bars representing SDs or as boxplots with median, upper and lower
294 quartiles (boxes) and percentiles (whiskers). Graphs were overlaid with the values of all individual
295 biological replicates. Linear regressions and survival curves show means and 95% confidence
296 intervals. Depending on results of normality testing, groups were compared using unpaired t test,
297 Mann-Whitney or One-Way Analysis of Variance with Tukey post-hoc test. Statistical significance is
298 indicated as * p <0.05, ** p <0.01, *** p <0.001, **** p <0.0001.

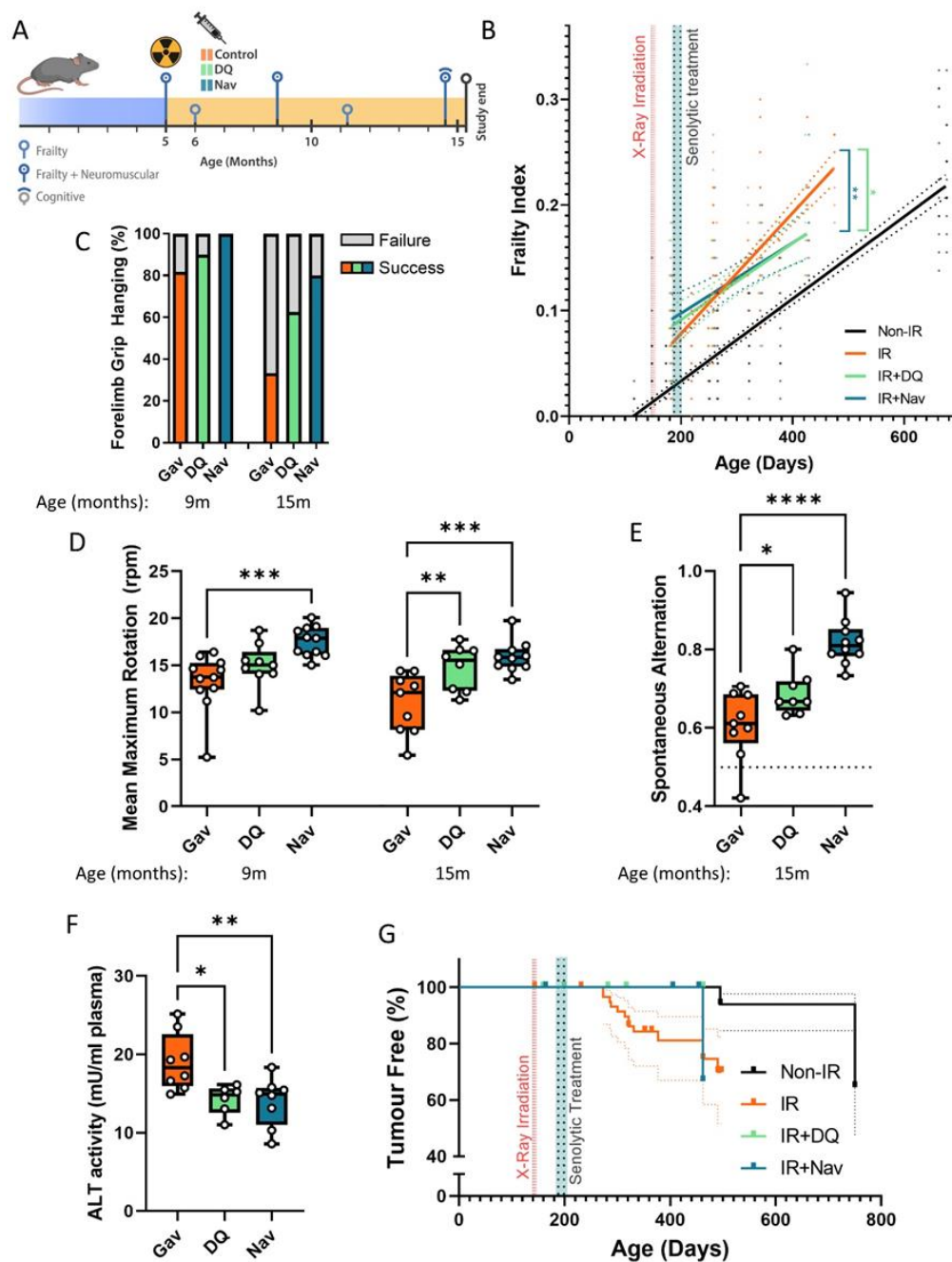
299

300

301 **Results**

302 **1. Short-term post-irradiation senolytic interventions rescue premature ageing**

303 Male C57Bl/6J mice received fractionated sub-lethal whole-body irradiation (IR, 3 x 3Gy) at an age of
304 5 to 6 months and were treated with a short course (10 days) of senolytics. Either 5mg/kg/day
305 Dasatinib + 50mg/kg/day Quercetin (D+Q) or 5 mg/kg/day Navitoclax, comparable to the lower
306 range of therapeutically used doses, by oral gavage at one month after irradiation, i.e. when acute
307 radiation sickness had abated (Fig. 1A). Irradiated mice experienced premature ageing as
308 documented by a doubling of the rate of frailty progression, decreased neuromuscular coordination,
309 decreased short-term memory and increased general and cancer-associated mortality ((Fielder et al.,
310 2019) and Fig. 1). When mice were treated with either senolytic drug at 1 month after IR indicators
311 of premature ageing were rescued over almost one year of follow-up (Figs. 1B – G). Although frailty
312 was not reversed, rates of frailty progression decreased after senolytic treatment to values
313 comparable to non-irradiated mice (Fig. 1B). The frailty index is composed of 30 different
314 assessments. Early intervention with each of the senolytics improved 6 of them, namely mouse
315 grimace scale, body condition, breathing rate, eye discharge/swelling, whisker loss and body weight
316 loss. In addition, Navitoclax treatment also reduced loss of fur colour and tumour incidence (Figure
317 1-figure supplement 1). Irradiated mice progressively lost neuromuscular coordination as indicated
318 by increasingly poorer performance in the wire hanging (Fig. 1C) and rotarod (Fig. 1D) tests.
319 Improvements for both interventions became greater with increasing age, with Navitoclax being
320 more effective than D+Q (Figs 1C, D). Short-term memory was assessed using spontaneous
321 alternation frequency in a Y-maze test at 16 months of age (Fielder et al., 2019). It was improved
322 substantially following Navitoclax treatment, with a modest improvement following D+Q (Fig. 1E).
323 Liver damage was assessed by the activity of alanine transaminase (ALT) and aspartate
324 aminotransferase (AST) in serum, which indicates leakage from hepatocytes, at 16 months of age.
325 ALT activity in serum was reduced under both interventions (Fig. 1F), suggesting that they enabled
326 better liver maintenance. However, intervention-dependent changes were not significant for AST
327 although ALT and AST activities were positively correlated amongst all mice (Correlation coefficient =
328 0.533, P=0.0000234). Picosirius Red staining did not show a significant effect of senolytics on liver
329 fibrosis. Although cohort sizes were not powered to assess long-term survival effects, both
330 treatments tended to result in improved survival and lower tumour prevalence at death in
331 comparison to irradiated control mice (Fig. 1G). While normal skin ageing is characterized by
332 epidermal thinning, irradiation-induced premature ageing is accompanied by hypertrophy of the
333 epidermis in the skin (Figure 1-figure supplement 2A,B). Neither D+Q nor Navitoclax treatment
334 reduced epidermal hypertrophy at late age (Figure 1-figure supplement 2C).



335

336 **Fig. 1: Short-term senolytic interventions rescue irradiation-induced accelerated ageing.**
 337 A) Layout of the experiment. B) Frailty index vs mouse age for non-irradiated (Non-IR, black),
 338 irradiated (IR, red), and irradiated plus treated with either D+Q (green) or Navitoclax (blue)
 339 mice. Irradiation and treatment times are indicated by vertical lines. Dots indicate FI for
 340 individual mice, regression lines and 95% confidence intervals are indicated by bold and
 341 dotted lines, respectively. C) Wire Hanging Test results (% success) under the indicated
 342 treatments and ages. D) Maximum speed achieved on Rotarod under the indicated
 343 treatments and ages. E) Short-term memory assessed as spontaneous alternation in a Y
 344 maze under the indicated treatments. F) ALT activity in plasma at 16 months. G) Tumour
 345 prevalence at death. Data are from 12 mice per group at start with attrition to 8-10 mice
 346 over the course of the experiment.

347

348

349 Sublethal irradiation resulted in persistently enhanced levels of markers for cellular senescence in
350 multiple tissues of mice for up to 12 months (Le et al., 2010; Seol et al., 2012). Senescence marker
351 levels in one year old irradiated mice were similar to those found in normally ageing mice older than
352 24 months (Hudgins et al., 2018; Jurk et al., 2014). We focused first on liver in which hepatocyte
353 senescence contributes causally to age-associated functional decline (Jurk et al., 2014; Ogrodnik et
354 al., 2017). As senescence markers, we measured nuclear size and karyomegaly (Aravinthan &
355 Alexander, 2016; Ogrodnik et al., 2017), nuclear HMGB1 exclusion (Davalos et al., 2013), nuclear
356 accumulation of Telomere-Associated DNA Damage Foci (TAF) and frequencies of TAF-positive
357 hepatocyte nuclei (Hewitt et al., 2012; Ogrodnik et al., 2017). Among TAF-positive cells, we assayed
358 both cells with any TAF and those with at least 3 TAF, because of previous evidence suggesting that
359 the latter might be more representative of cells in 'full' or 'late' senescence (Zou, Sfeir, Gryaznov,
360 Shay, & Wright, 2004) (Jurk et al., 2014). The markers indicated higher frequencies of senescent
361 hepatocytes at 7 months after irradiation (Figure 1-figure supplement 3A-F). Marker changes were
362 similar to those seen in normally ageing mice at ages above 30 months (Figure 1-figure supplement
363 3G-K). Navitoclax intervention at 6 months of age resulted in reduced senescent hepatocyte
364 frequencies in liver 10 months later as indicated by all markers tested (Figure 1-figure supplement
365 4A-F). However, D+Q intervention led to reduced nuclear size and hepatocyte karyomegaly but did
366 not maintain a significant long-term reduction of HMGB1-negative or TAF-positive hepatocytes
367 (Figure 1-figure supplement 4A-F).

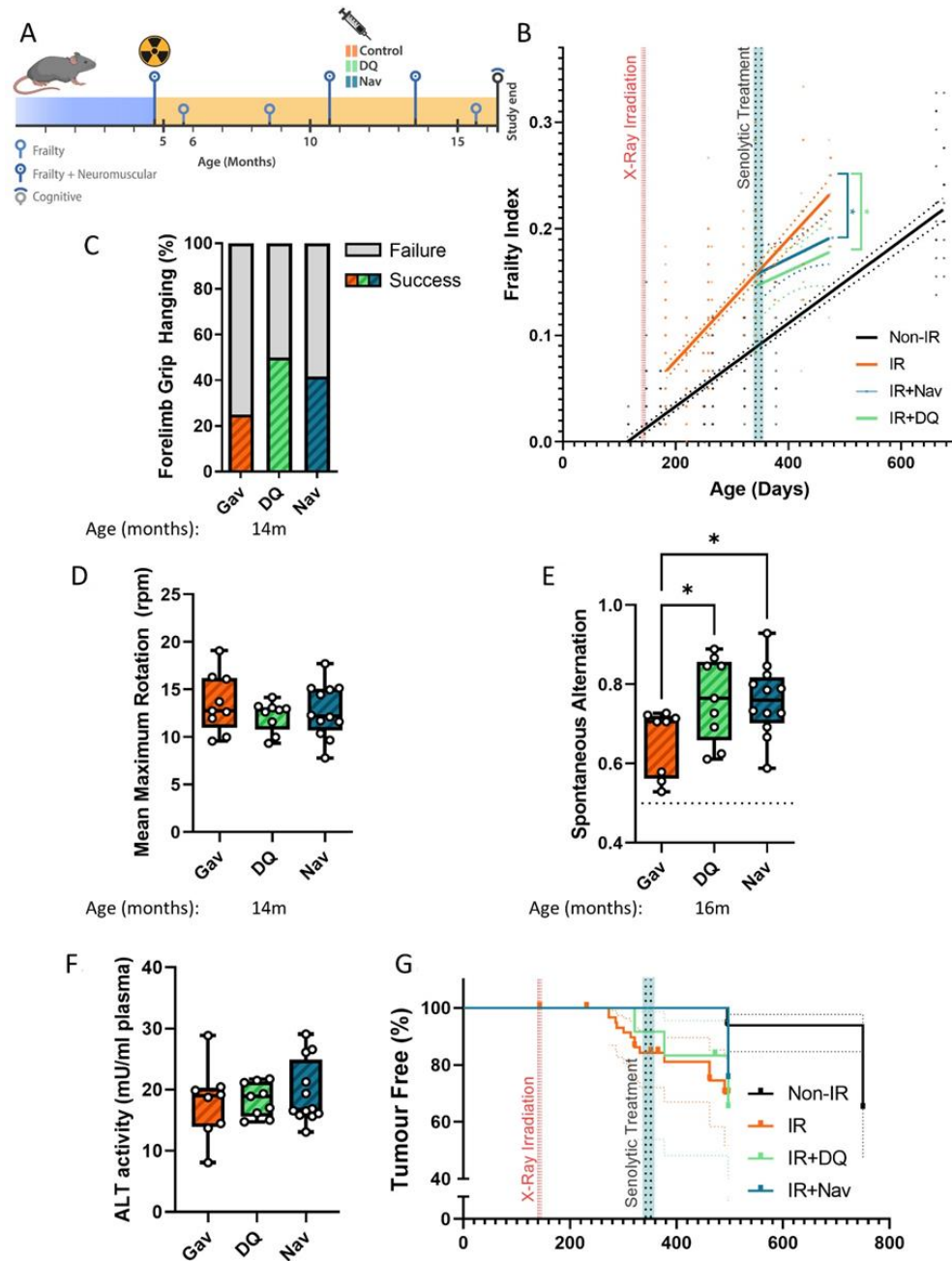
368 Senescent cell burden, specifically in the hippocampus, is associated with memory deficits in ageing
369 mice (Fielder et al., 2020; Musi et al., 2018; Ogrodnik et al., 2021). To assess the mechanistic basis
370 for the observed improvements of short-term memory (Fig. 1E), we measured markers for a
371 senescence-like phenotype (nuclear size, loss of nuclear Lamin B1 expression and TAF frequencies)
372 and for neuroinflammation (ionized calcium-binding adapter molecule 1 (Iba1)-positive cell density
373 and soma size) in the CA1 and CA3 hippocampal regions (Figure 1-figure supplement 5). Both D+Q
374 and Navitoclax reduced nuclear size (Figure 1-figure supplement 5A,B) and TAF frequencies (Figure
375 1-figure supplement 5E-I) as markers for a senescent phenotype in CA1 and CA3 pyramidal layer
376 neurons, but Navitoclax had no effect on laminB1 expression (Figure 1-figure supplement 5C,D).
377 Similarly, Navitoclax had no effect on frequencies of Iba1-positive microglia (Figure 1-figure
378 supplement 5J,K), although microglia soma size was reduced in CA1 and CA3 after both treatments
379 (Figure 1-figure supplement 5L,M).

380 We also examined the effects of D+Q or Navitoclax treatment on morphological and functional
381 parameters of hind limb muscle (Figure 1-figure supplement 6). Interestingly, improvements of
382 neuromuscular coordination (Fig. 1C) and strength/endurance (Fig. 1D) were not associated with
383 enhanced muscle fibre diameter (Figure 1-figure supplement 6A,B), decreased frequency of p21-
384 positive myonuclei (Figure 1-figure supplement 6C,D) or decreased frequency of TAF-positive
385 myonuclei (Figure 1-figure supplement 6E) as senescence marker. Neither irradiation alone or
386 combination with either of the senolytic interventions changed hind limb muscle fibrosis or fat
387 accumulation as assessed by Picro-SiriusRed/FastGreen staining.

388

389 **2. Late senolytic interventions block further progression of irradiation-induced premature
390 ageing**

391 So far, our data showed that a short senolytic intervention at an early timepoint can rescue
392 irradiation-induced premature accumulation of senescent cells as well as premature physiological
393 ageing. We next asked the question, whether senolytics could still be effective if mice were treated
394 late after irradiation, when premature ageing was already manifest. Animals were again irradiated at
395 5 months of age, but senolytic interventions were delayed for 6 months and mice were treated with
396 the senolytics D+Q or Navitoclax (using the same regimen as before) at 11 months of age (Fig. 2A). At
397 this timepoint, the frailty index in irradiated mice was already significantly above that in sham-
398 irradiated mice (Fig. 2B). However, similar to early intervention, late senolytic treatment did not
399 reduce the frailty index score, but rescued its further accelerated progression (Fig. 2B). Late
400 intervention with each of the senolytics improved largely the same components of the frailty index
401 as early senolytic intervention, namely mouse grimace scale, body condition, breathing rate, and eye
402 discharge/swelling (Figure 1-figure supplement 1). Mice that had been treated with senolytics at 11
403 months of age still showed a tendency for improved results of the hanging wire test at 14 months
404 (Fig. 2C), however, rotarod performance was not better than in irradiated animals (Fig. 2D). Late
405 intervention with either senolytic improved short-term memory at late age (Fig. 2E). Neither liver
406 damage (Fig. 2F) nor tumour incidence (Fig. 2G) following late senolytic treatment was significantly
407 reduced. Epidermal thickness was unchanged (Figure 2-figure supplement 1).



408

409 **Fig. 2: Late senolytic interventions partially block further progression of irradiation-**
 410 **induced accelerated ageing.** A) Layout of the experiment. B) Frailty index vs mouse age for
 411 non-irradiated (Non-IR, black), irradiated (IR, red), and irradiated plus treated with either
 412 D+Q (green) or Navitoclax (blue) mice. Irradiation and treatment times are indicated by
 413 vertical lines. Dots indicate FI for individual mice, regression lines and 95% confidence
 414 intervals are indicated by bold and dotted lines, respectively. C) Wire Hanging Test results (%
 415 success) under the indicated treatments. D) Maximum speed achieved on Rotarod under the
 416 indicated treatments at 14 months of age. E) Short-term memory assessed as spontaneous
 417 alternation in a Y maze under the indicated treatments. F) ALT activity in serum, 16 months
 418 old. G) Tumour prevalence at death. Data are from 12 mice per group at start with attrition
 419 to 8-10 mice over the course of the experiment.

420

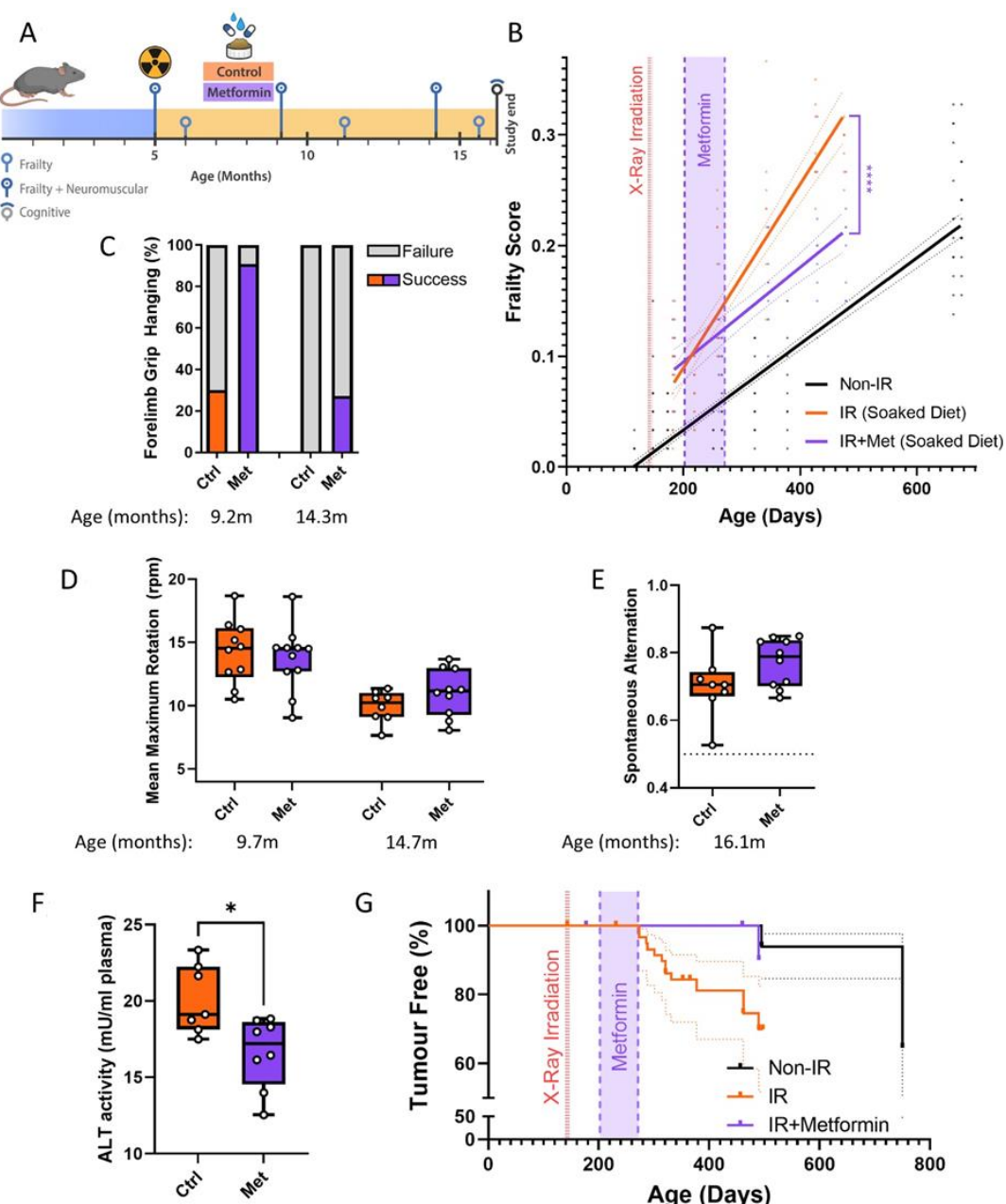
421 In agreement with a diminished effect of late treatments on liver damage, there was also less impact
422 on persistent systemic cell senescence as assessed by TAF frequencies in liver (Figure 2-figure
423 supplement 2D-F), however, treatment with Navitoclax still reduced nuclear size (Figure 2-figure
424 supplement 2A), karyomegaly (Figure 2-figure supplement 2B) and frequencies of HMGB1-negative
425 hepatocytes (Figure 2-figure supplement 2C) suggesting a reduced senescent burden. There was no
426 improvement of hind limb myofibre cross sectional area but rather a tendency (significant for
427 Navitoclax) to reduce it (Figure 2-figure supplement 3A,B). There was no reduction of TAF
428 frequencies in muscle (Figure 2-figure supplement 3C). However, in agreement with improved
429 memory maintenance (Fig 2E) we found a reduction of neuroinflammation markers in the CA1 (both
430 markers) and CA3 (microglia soma size only) regions of the hippocampus following both late
431 interventions (Figure 2-figure supplement 4).

432 Together, these data show that a short-term senolytic intervention even if applied at an advanced
433 age still has beneficial effect on irradiation-induced premature progression of frailty and cognitive
434 decline.

435

436 **3. A short-term intervention with the senostatic metformin rescues irradiation-induced
437 premature ageing**

438 Senolytics can have serious side effects, for instance Navitoclax-induced thrombocytopenia at higher
439 doses (Demaria, 2017), that may be limiting for preventive applications. Senostatic or senomorphic
440 caloric restriction mimetics, which block senescence-stabilizing signalling, can also reduce net
441 accumulation of senescent cells in tissues (da Silva et al., 2019; C. Wang et al., 2010). One example is
442 metformin, which has been shown to act as a senostatic (Moiseeva et al., 2013) and has an excellent
443 safety profile as testified by about 70 years of clinical application. We therefore decided to treat our
444 irradiated mice with metformin for a relatively short period (10 weeks), starting at one month after
445 irradiation, and assessed the long-term effects of this treatment (Fig. 3A). Similar to senolytic
446 interventions, metformin treatment rescued the enhanced rate of frailty progression due to
447 irradiation (Fig. 3B). Among the components of frailty, metformin improved mouse grimace scale,
448 body condition, breathing rate, whisker loss and body weight loss at late age (Figure 1-figure
449 supplement 1). It also improved neuromuscular coordination as tested by hanging wire test (Fig.
450 3C), but had only a minor effect on performance on the rotarod at late age (Fig. 3D), which might be
451 due to the high body weights of mice fed soaked food. At 16 months of age, metformin-treated
452 animals tended to perform better in the short term memory test (Fig. 3E), showed less liver damage
453 (Fig. 3F) and tumour prevalence at death was reduced to the levels as in sham-irradiated mice (Fig.
454 3G). Metformin treatment also tended to reduce irradiation-induced epidermal hypertrophy
455 assessed at 16 months of age (Figure 3-figure supplement 1).



456

457 **Fig. 3: A short-term intervention with the senostatic metformin rescues irradiation-**
 458 **induced accelerated ageing.** A) Outline of the experiment. Animals were irradiated at 5
 459 months of age and treated with either soaked food (controls) or metformin in soaked food
 460 (Met) from 6 months of age for 10 weeks. B) Frailty index vs mouse age for non-irradiated
 461 (no IR, black), irradiated (IR, red), and irradiated plus treated with metformin (blue) mice.
 462 Irradiation and treatment times are indicated by vertical lines. Dots indicate FI for individual
 463 mice, regression lines and 95% confidence intervals are indicated by bold and dotted lines,
 464 respectively. C) Wire Hanging Test results (% success) under the indicated treatments and
 465 ages. D) Maximum speed achieved on Rotarod under the indicated treatments and ages. E)
 466 Short-term memory assessed as spontaneous alternation in a Y maze under the indicated
 467 treatments. F) ALT activity in plasma at 16 months of age. G) Tumour prevalence at death.
 468 Data are from 12 mice per group at start with attrition to 8-10 mice over the course of the
 469 experiment.

470

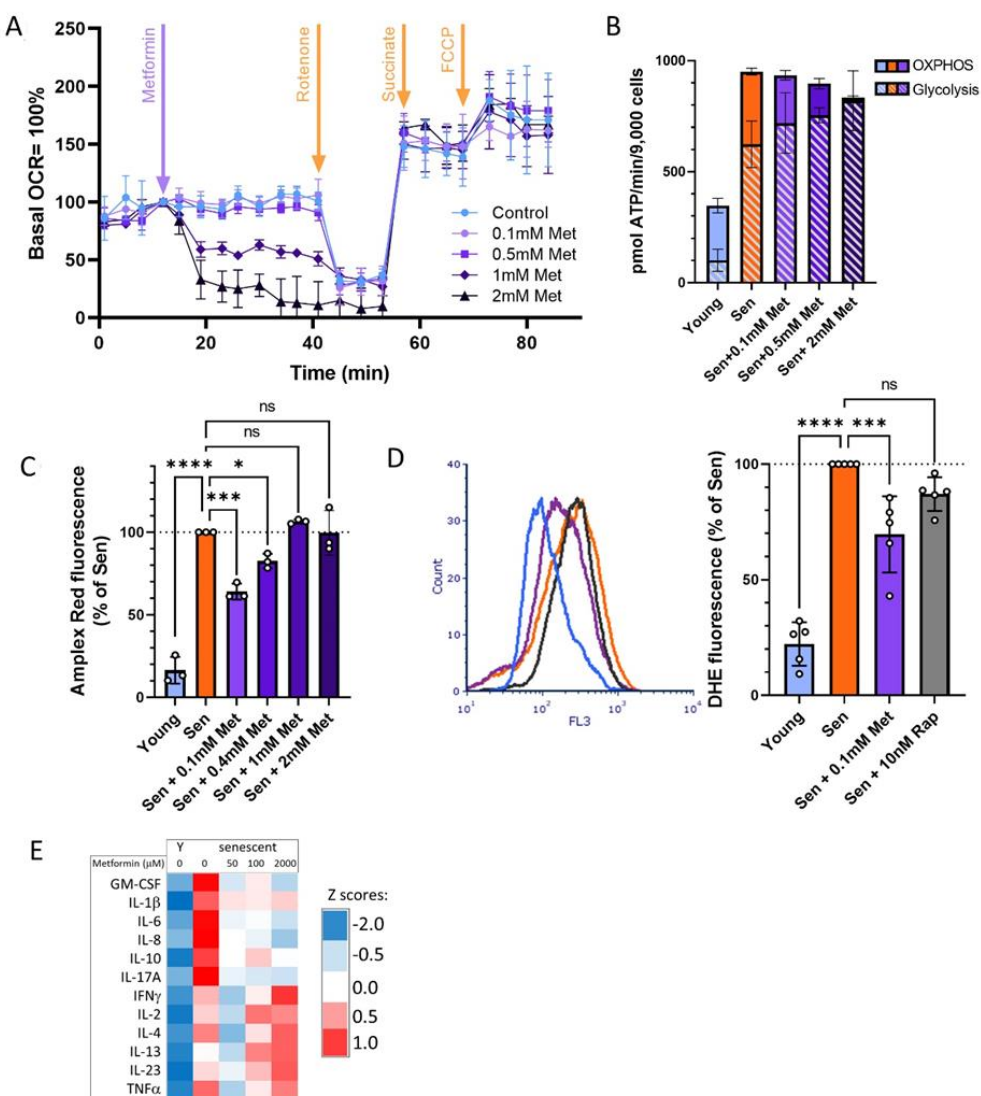
471 All tested senescence markers in livers of metformin-treated mice indicated the reduction of
472 senescent cell frequencies at old age (16 months) (Figure 3-figure supplement 2A-F). Similarly,
473 senescence and neuroinflammation markers in the CA1 and CA3 regions of the hippocampus were
474 deceased (Figure 3-figure supplement 3A-F). Interestingly, metformin treatment improved skeletal
475 muscle fibre maintenance as shown by larger cross-sectional area of both oxidative and non-
476 oxidative muscle fibres (Figure 3-figure supplement 4A,B) and reduced TAF frequencies in myocyte
477 nuclei (Figure 3-figure supplement 4C).

478 In conclusion, these data indicate that a relatively short treatment with the senostatic metformin
479 rescues multiple domains of irradiation-induced premature ageing in mice for at least 10 months
480 after cessation of the intervention.

481

482 **4. At therapeutic concentrations, metformin inhibits the SASP by reducing NOX4 activity in
483 senescent cells**

484 Metformin can block the SASP, and thus act as a senostatic, by inhibiting complex I of the electron
485 transport chain, thus causing a reduction of mitochondrial ROS production, which in turn will reduce
486 the activity of the NF- κ B transcription factor, the major driver of the pro-inflammatory SASP. This
487 pathway has been identified *in vitro*, using millimolar concentrations of metformin (Moiseeva et al.,
488 2013). However, therapeutically achievable metformin concentrations in the vast majority of tissues
489 in mice or man are typically well below 100 μ M (Wilcock & Bailey, 1994). In permeabilised human
490 fibroblasts *in vitro*, metformin inhibits complex I-dependent respiration with pyruvate and malate in
491 concentrations around 1 mM or higher but has no detectable effect on oxygen consumption rates at
492 100 μ M (Fig. 4A). Supplementation of the complex II substrate succinate completely restored
493 respiration under metformin, confirming that metformin at high concentrations inhibits complex I
494 specifically (Fig. 4A). Even when senescent human fibroblasts were treated with various
495 concentrations of metformin for 10 days to mimic longer term *in vivo* interventions, low metformin
496 concentrations (100 μ M) did not decrease mitochondria dependent ATP production compared with
497 senescent untreated controls. In contrast, 2 mM metformin shifted cellular ATP production almost
498 entirely to glycolysis with little contribution from mitochondrial oxidative phosphorylation (Fig. 4B).
499 Interestingly, the senescence-associated enhanced H₂O₂ production from whole cells (as measured
500 by Amplex Red assay) was rescued only by low (up to 400 μ M), but not by high metformin
501 concentrations (Fig. 4C). Reduction of ROS production in senescent cells by long-term treatment
502 with low metformin concentrations was confirmed by measuring cellular ROS levels using DHE
503 fluorescence (Fig. 4D), with a stronger effect for metformin as compared to rapamycin. In
504 accordance with the ROS data (Figs. 4C, D), low concentrations of Metformin were more effective
505 than higher ones in reducing a wider range of cytokines in the secretome of senescent fibroblasts
506 (Fig. 4E). Together, these data indicate that low, therapeutically relevant concentrations of
507 metformin reduce the release of ROS and SASP cytokines from senescent cells, which can explain the
508 senostatic activity of metformin *in vivo*. Importantly, this effect was not mediated by complex I
509 inhibition.

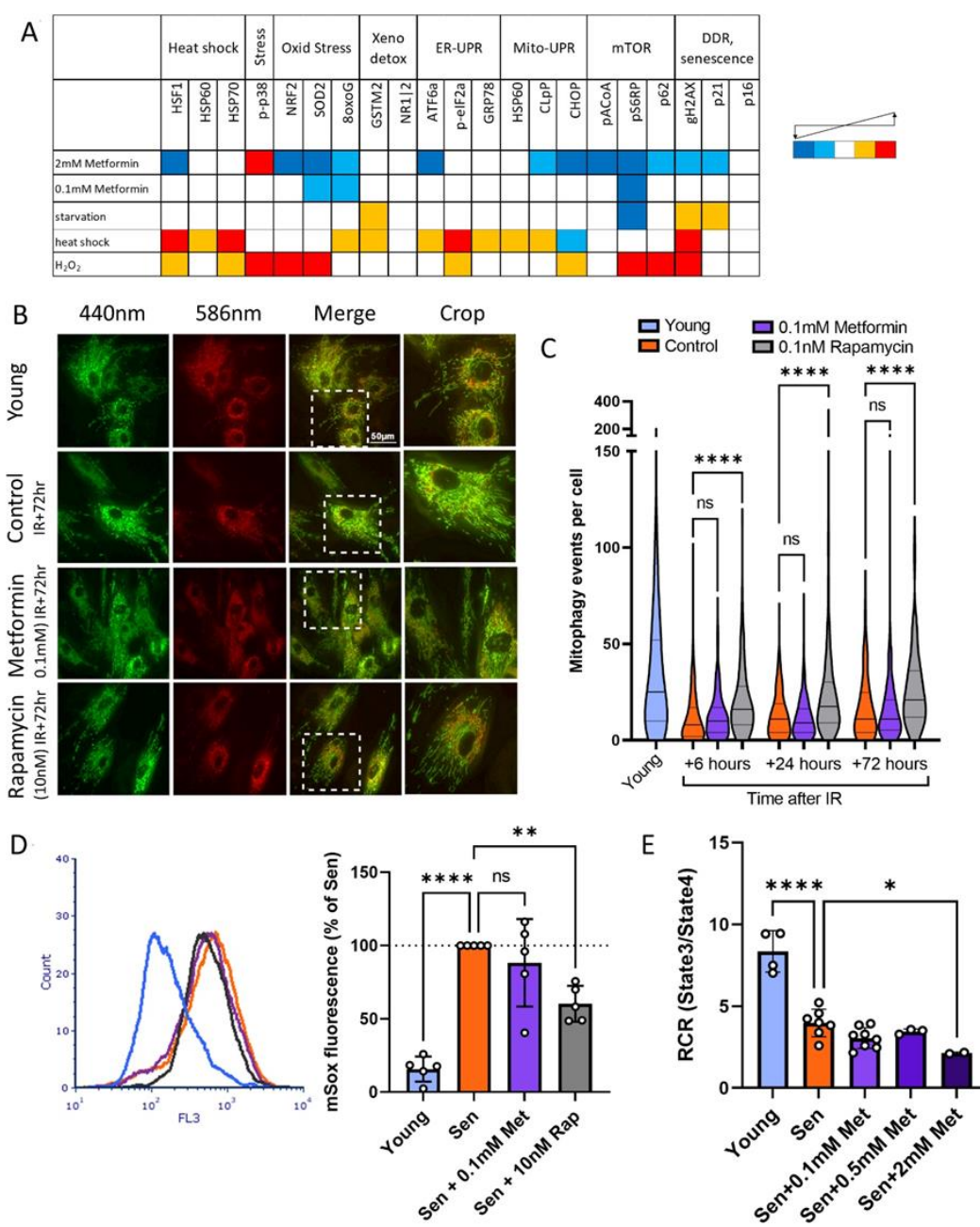


510

511 **Fig. 4. At therapeutic concentrations, metformin reduces ROS and SASP but by**
 512 **inhibition of complex I.** A) Mitochondrial oxygen consumption rate of permeabilised MRC5
 513 human fibroblasts treated sequentially (at timepoint indicated by arrow) with various
 514 concentrations of metformin (Met), 0.5μM rotenone (Rot), 4mM Succinate (Suc) and 2.5μM
 515 FCCP. M± SD, n=4. B) ATP production rate by Oxidative phosphorylation (OXPHOS)
 516 and glycolysis in young and senescent MRC5 human fibroblasts treated for 10 days with the
 517 indicated metformin concentrations. M± SD, n=4. C) Impact of metformin in the indicated
 518 concentrations on ROS production measured by AR in human fibroblasts. Cells were induced
 519 to senescence by IR and treated with metformin for 10 days. M± SD, N=3. D) Impact of
 520 rapamycin and metformin on ROS levels in human fibroblasts measured by DHE fluorescence
 521 in FACS. Left: representative FL3 histograms. Light blue: young, red: senescent (10d past IR),
 522 purple: senescent + 0.1mM metformin, black: senescent + 10nM rapamycin. Right: Average
 523 DHE fluorescence intensities. M± SD, n=5. E) Cytokine concentrations in the supernatant of
 524 human fibroblasts. N= 2. Senescent fibroblasts were treated with the indicated metformin
 525 concentrations for 10 days.

526

527 To identify potential alternative mechanisms of the senostatic activity of metformin, we subjected
528 human fibroblasts treated with either low (100 μ M) or high (2 mM) metformin concentrations to a
529 stress response pathway identifier assay by cytometry by time of flight (CyTOF). Two or three
530 antigens were chosen to represent each of seven cellular stress response pathways, namely heat
531 shock, oxidative stress response, xenobiotics response, ER-UPR, Mito-UPR, nutrient signalling
532 pathway/autophagy and DNA damage response(DDR)/senescence, resulting in a panel of 21
533 antibodies (Table 2). Cells were treated with test interventions for 2 days and analysed by CyTOF
534 using the antibody panel. Starvation, heat shock and oxidative stress by H_2O_2 treatment were used
535 as positive control interventions. In the positive control experiments, activation of heat shock and
536 oxidative stress response pathways were evident following the respective control treatments
537 together with induction of autophagy and a DDR/senescence, while starvation impacted primarily
538 onto the mTOR pathway, together validating the assay (Fig. 5A). Treatment with high metformin
539 reduced the levels of marker proteins in a wide range of pathways, including heat shock, oxidative
540 stress response, ER-UPR, Mito-UPR, nutrient signalling pathway/autophagy and DDR/senescence. In
541 contrast, low metformin only reduced indicators of oxidative stress response as expected (compare
542 Figs. 4C, D) and nutrient signalling (Fig. 5A). This suggested that low metformin might activate
543 autophagy and mitophagy via suppression of the mTOR pathway and thus contribute to a reduction
544 of mitochondrial ROS production in senescence. Therefore, we next examined mitophagy activity in
545 human fibroblasts transfected with the mitophagy reporter mt-mKeima (Katayama, Kogure,
546 Mizushima, Yoshimori, & Miyawaki, 2011), which localises to mitochondria and displays a shift in
547 fluorescence emission under low pH, when mitochondria are delivered into lysosomes (indicated in
548 red, Fig. 5B). As shown before (Dalle Pezze et al., 2014; Korolchuk, Miwa, Carroll, & von Zglinicki,
549 2017), mitophagy activity was reduced in senescent cells. This reduction occurred within hours after
550 irradiation and mitophagy remained low in irradiated cells for multiple days (Fig. 5C). Treatment with
551 rapamycin improved mitophagy at all time points, but 100 μ M metformin had no effect (Fig.5C).
552 Mitochondrial dysfunction in senescence is characterized by high ROS production together with low
553 respiratory coupling (Passos et al., 2007). In accordance with their effects on mitophagy, rapamycin,
554 but not metformin, suppressed senescence-associated mitochondrial superoxide production as
555 measured by MitoSOX fluorescence (Fig. 5D). Moreover, metformin did not rescue mitochondrial
556 dysfunction in senescent cells as assessed by respiratory control ratio with the complex I-linked
557 substrate, pyruvate+malate (Fig. 5E).

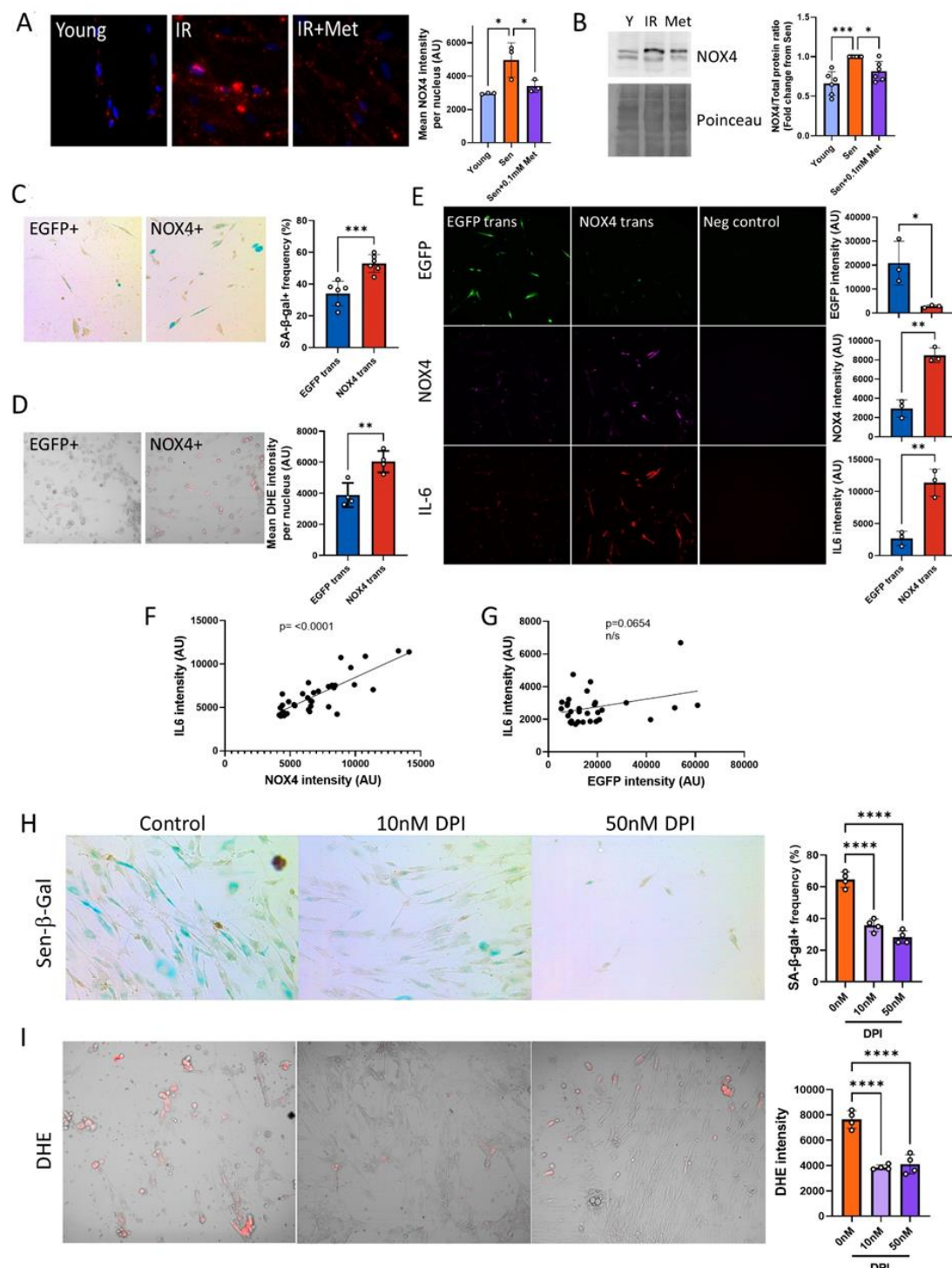


558

559 **Fig. 5. Low concentrations of metformin do not improve mitochondrial turnover and**
 560 **function.** A) Impact of high (2mM) and low (100 μ M) concentrations of metformin on stress
 561 response pathways in human fibroblasts. CyTOF with the indicated antibodies was
 562 performed on human MRC5 fibroblasts treated for 2 days with the indicated interventions.
 563 Heat map colour codes indicate strong decrease (dark blue), mild decrease (light blue), no
 564 change (white), light increase (amber) or strong increase (red) as exemplified in Figure 5-
 565 figure supplement 1. Data are pooled from two independent experiments. B) Dermal
 566 fibroblasts expressing mt-mKeima were irradiated with 20Gy and treated with either 100 μ M
 567 Metformin or 10nM Rapamycin for 3 days. Red fluorescence indicates mitochondria
 568 engulfed in lysosomes. C) Number of mitophagy events per cell. Dermal fibroblasts
 569 expressing mt-mKeima were irradiated with 20Gy and treated with either 100 μ M Metformin

570 or 10nM Rapamycin for the indicated times. N= 196 – 271 cells per condition pooled from 3
571 biological repeats. D) Impact of rapamycin and metformin on mitochondrial superoxide
572 levels in human fibroblasts either young or at 10d after IR measured (Sen) by MitoSOX
573 fluorescence in FACS. N=5. E) Respiratory Control Ratio (RCR) of mitochondria in fibroblasts
574 at 10d after IR treated with the indicated concentrations of metformin. N≥3.
575

576 Together, these data suggested that low metformin has no effect on mitochondrial (dys)function in
577 senescence. Therefore, we tested the alternative possibility that it might primarily reduce non-
578 mitochondrial, rather than mitochondrial, ROS production in senescent cells. ROS production by the
579 NADPH oxidase 4 (NOX4) has been shown to contribute to replicative (Lener et al., 2009), oncogene-
580 induced (Weyemi et al., 2012) and stress-induced senescence (Goy et al., 2014) although its knock-
581 out had no impact on lifespan in mice (Rezende et al., 2017). To test the hypothesis that low
582 metformin might act as a senostatic via reduction of the major cytoplasmic ROS generator NOX4, we
583 first measured the abundance of NOX4 in senescent fibroblasts, which was enhanced as expected
584 (Fig. 6A, B). Moreover, NOX4 did not colocalise with mitochondria (Figure 6-figure supplement 1). A
585 low concentration of metformin (100 μ M) reduced NOX4 protein levels in senescent human
586 fibroblasts as shown by both immunofluorescence (Fig. 6A) and Western blotting (Fig. 6B). To test
587 whether manipulation of NOX4 alone would be sufficient to explain the senostatic activity of
588 metformin, we over-expressed NOX4 in young fibroblasts and assessed its effects on markers of
589 senescence, SASP and ROS. In comparison to EGFP-overexpressing controls, NOX4-overexpressing
590 fibroblasts were more often positive for Sen- β -Gal (Fig. 6C) and produced higher levels of ROS (Fig.
591 6D). Importantly, cells overexpressing NOX4 produced significantly more of the SASP interleukin IL-6
592 (Fig. 6E), and there was a strong positive correlation between NOX4 and IL-6 levels (Fig. 6F), but not
593 between EGFP and IL-6 (Fig. 6G). Finally, we treated fibroblasts in stress-induced senescence with
594 the NADPH oxidase inhibitor Diphenyleneiodonium chloride (DPI), which reduced both Sen- β -Gal
595 activity as a marker for the senescent phenotype (Fig 6H) and DHE fluorescence, indicative of
596 decreased production of senescence-associated ROS (Fig 6I).



597

598 **Fig. 6. Low concentrations of metformin reduce ROS in senescence via suppression of NOX4. A)**
599 Human fibroblasts were irradiated with 20Gy and treated with 100μM Metformin for 10 days. Left:
600 representative images of cells treated as indicated, red: NOX4 immunofluorescence, Blue: DAPI.
601 Right: Quantification of NOX4 fluorescence intensity. B) Left: Representative NOX4 Western blot.
602 Cells treated as above. Right: Average NOX4 signal intensity, normalised to total protein. C) Left:
603 Sen-β-Gal staining in EGFP- and NOX4-overexpressing fibroblasts. Right: Average frequencies of Sen-
604 β-Gal-positive cells. D) Left: DHE staining in EGFP- and NOX4-overexpressing fibroblasts. DHE
605 fluorescence in red, cells visualised in phase contrast. Right: Average DHE fluorescence intensity per

606 cell. E) Co-staining for NOX4 (red) and IL-6 (green) on EGFP- or NOX4-transfected fibroblasts. Right:
607 Fluorescence intensity levels for EGFP (top), NOX4 (middle) and IL-6 in EGFP- and NOX4-transfected
608 cells. F) Correlation between cellular NOX4 and IL6 fluorescence signals in NOX4-transfected cells. G)
609 Correlation between cellular EGFP and IL6 fluorescence signals in EGFP-transfected cells. H) Left:
610 Sen- β -Gal staining in senescent fibroblasts treated with the indicated concentrations of DPI. Right:
611 Frequencies of Sen- β -Gal-positive cells. I) Left: DHE staining in senescent fibroblasts treated with the
612 indicated concentrations of DPI. DHE fluorescence in red, cells visualised in phase contrast. Right:
613 Average intensity of DHE fluorescence per cell. All experiments N \geq 3.

614

615 Together, our data indicate that metformin at low, therapeutically achievable concentrations
616 reduces senescence-associated ROS production by diminishing NOX4 abundance in senescent cells,
617 which in turn causes the reduction of other facets of the senescent phenotype, importantly including
618 a reduction of SASP production.

619

620 Discussion

621 Irradiation is a mainstay of successful therapy for the vast majority of cancers. However, sublethal
622 irradiation causes progressive, premature frailty in both humans (Ness et al., 2018; Robison &
623 Hudson, 2014) and mice (Fielder et al., 2019). Frailty is a medical syndrome characterised by system-
624 wide decreased physiological reserves and thus increased vulnerability (Rockwood, Mitnitski, &
625 Howlett, 2015) predicting multimorbidity and mortality in humans (Kojima, Iliffe, & Walters, 2018)
626 and mice (Whitehead et al., 2014). In long-term tumour survivors, frailty prevalence reaches a level
627 equal to the general population of 60 – 70 year olds about 30 years earlier (Ness et al., 2013), and in
628 mice frailty progression after sublethal whole-body irradiation is about twice as fast as in non-
629 irradiated animals (Fielder et al., 2019). Together with multimorbidity and increased mortality,
630 greatly enhanced frailty is a major component of a serious premature ageing phenotype in long-term
631 tumour survivors, for which no treatment is available so far.

632 Adjuvant senolytic intervention can relieve some of the consequences of experimental irradiation or
633 chemotherapy in mice. For instance, pharmacogenetic or pharmacologic senolytic intervention up to
634 12 weeks after irradiation or treatment with the radiation mimetic doxorubicin (partially) corrected
635 treatment-induced loss of immune function (Chang et al., 2016; Palacio et al., 2019), bone loss
636 (Chandra et al., 2020), cardiac dysfunction and loss of physical activity (Demaria et al., 2017) and
637 liver damage (Baar et al., 2017). However, whether an adjuvant senolytic intervention would be able
638 to rescue organism-wide radiation-induced premature ageing as documented by frailty levels has
639 not been shown before. Moreover, there is very little data addressing the possible persistence of
640 beneficial effects of senolytic interventions; most published experiments test the outcomes of
641 senolytic treatments only within days to weeks after the intervention. We are only aware of a single
642 paper (Zhu et al., 2015) showing that a beneficial effect of a treatment with D+Q (improvement of
643 muscle strength in an irradiated mouse leg) could last for up to 7 months.

644 Our core hypothesis was that therapy-induced senescence would greatly and persistently accelerate
645 the accumulation of senescent cells by enhancing secondary senescence via bystander signalling,
646 thus causing progressive worsening of ageing-associated symptoms with time following a single bout
647 of DNA-damaging therapies (Short et al., 2019). If this hypothesis is correct, eliminating therapy-
648 induced senescent cells by a one-off, short senolytic or senostatic intervention adjuvant to radiation-

649 or chemotherapy should be sufficient to prevent progressive premature ageing and to normalise the
650 rate of frailty progression.

651 Our data support this hypothesis. A single, relatively short adjuvant intervention with either
652 senolytic or the senostatic metformin rescued the radiation-induced accelerated progression of
653 multi-system frailty for at least almost one year. We started the interventions at one month after
654 completion of radiation, i.e. when signs of acute radiation sickness in the mice had abated but levels
655 of radiation-induced senescence in many tissues were still not significantly above controls (Mylonas
656 et al., 2021; Palacio et al., 2019; Palacio, Krishnan, Le, Sharpless, & Beausejour, 2017). That this was
657 sufficient to cause a significant reduction of senescence markers in tissues like liver and brain 10
658 months later is again in agreement with a central role of bystander-mediated accelerated
659 progression of senescence following irradiation.

660 When senolytic interventions were performed only after enhanced frailty was established, beneficial
661 long-term effects were reduced. There was no longer an effect on muscular or liver function and
662 little improvement on senescence markers in liver at old age. Similarly, Mylonas et al. (Mylonas et
663 al., 2021) recently reported that a late intervention with Navitoclax reduced senescence markers in
664 kidney but did not improve kidney fibrosis. However, late interventions were still efficient in rescuing
665 further frailty progression and liver maintenance and tended to improve short-term memory at high
666 age consistent with a significant reduction of markers for neuroinflammation. This confirms recent
667 data (Yabluchanskiy et al., 2020) showing improvements of brain senescence markers, neurovascular
668 coupling and memory after relatively late (3 months past whole brain irradiation) pharmacogenetic
669 (ganciclovir in 3MR mice) or Navitoclax intervention. Our results might be interpreted to suggest that
670 ongoing brain cell senescence, including neuron senescence, could be a physiologically relevant
671 driver of neuroinflammation.

672 While senolytic drugs work in principle on a systemic level, their senolytic activity is cell type-
673 specific. For instance, Navitoclax has senolytic activity against HUVECs and fibroblasts, but not
674 adipocytes *in vitro* (Zhu et al., 2016), while D+Q in combination eliminated senescent HUVECs,
675 fibroblasts and fat progenitor cells (Zhu et al., 2015). The specific activity of these senolytics against
676 many other senescent cell types is not known. Our data show cell type-specific differences in the
677 capacity of Navitoclax vs D+Q for long-term reduction of senescence markers *in vivo*: under an early
678 intervention regime, Navitoclax and D+Q reduced hippocampal pyramidal neuron senescence at late
679 age equally well but had no effect on senescence marker in muscle fibres, while senescence markers
680 in liver hepatocytes were only efficiently reduced by Navitoclax but not by D+Q. This pattern was
681 different from the physiological responses in the same tissues: Navitoclax and D+Q improved
682 function in the liver (as measured by ALT release), brain (short-term memory) and muscle (rotarod
683 and hanging wire performance) with only a slightly better performance of Navitoclax in terms of
684 memory and muscle function. The senostatic metformin might be expected to have less cell type
685 specificity, and in fact it did reduce late age senescent cell frequencies both in liver, brain and
686 muscle. Together, these data suggest that cognitive improvement by senolytics could be tissue-
687 autonomous, but that there must be significant contributions from systemic effects causing
688 improvements in muscular and possibly liver function. However, measuring the serum abundance of
689 18 major interleukins at late age, we did not find evidence for obvious impacts of any of the
690 interventions, suggesting that the mediation of systemic effects might be more complex than
691 persistent suppression of some pro-inflammatory cytokines.

692 The capacity of the dietary restriction mimetic metformin to extend lifespan and healthspan in mice
693 (Martin-Montalvo et al., 2013) and probably man (Campbell, Bellman, Stephenson, & Lisy, 2017; C.
694 P. Wang, Lorenzo, Habib, Jo, & Espinoza, 2017) is well documented. Among other mechanisms,

695 metformin, like dietary restriction itself (da Silva et al., 2019), inhibits the pro-inflammatory SASP
696 (Moiseeva et al., 2013) and thus limits the spread of senescence via bystander effects. We therefore
697 expected it to be similarly effective as senolytics in reducing persistent therapy-induced senescence
698 and its physiological consequences, and our results confirmed this expectation.

699 It has been shown that metformin inhibits complex I of the mitochondrial electron transport chain,
700 thus reducing ROS production (Moiseeva et al., 2013). ROS levels are high in senescent cells (Passos
701 et al., 2010; Passos et al., 2007) and their ability to activate the SASP is well documented (Coppe,
702 Desprez, Krtolica, & Campisi, 2010; Nelson, Kucheryavenko, Wordsworth, & von Zglinicki, 2018).
703 Thus, it has been suggested that metformin diminishes the SASP via complex I inhibition (Moiseeva
704 et al., 2013). However, metformin inhibits complex I only at supraphysiological concentrations. At
705 therapeutically achievable and effective concentrations, it still reduces cellular ROS (Fig. 4C, D) and
706 the SASP (Fig. 4E), but has no effect on mitochondrial complex I-linked oxygen consumption (Fig. 4A,
707 B).

708 Complex I is a multiprotein enzyme consisting of more than 40 subunits. In ageing and cellular
709 senescence, incompletely assembled subcomplexes of complex I accumulate and contribute to
710 cellular ROS production (Miwa et al., 2014). Decreased efficacy of mitophagy in senescence and
711 ageing is a possible cause of this accumulation (Dalle Pezze et al., 2014; Korolchuk et al., 2017).
712 Therefore, we next tested whether metformin at therapeutic concentrations might be able to rescue
713 the low mitophagy activity in senescence, using rapamycin as a positive control. Surprisingly, low
714 metformin concentrations did not improve mitophagy (Fig. 5B, C). In agreement with this, they did
715 not reduce mitochondrial ROS production as measured by MitoSOX fluorescence (Fig 5D) and did not
716 rescue low mitochondrial coupling (Fig. 5E) in senescence, suggesting a non-mitochondrial pathway
717 for reduction of ROS by therapeutic metformin concentrations. Suppression of NOX4 was identified
718 as a mechanism by which low metformin reduces senescence-associated ROS production and SASP
719 (Fig. 6). It had been shown that metformin suppresses NOX4 induction via activation of AMPK both
720 at concentrations as high as 10 mM (Sato et al., 2016) and as low as 0.1 mM (Shi & Hou, 2021).
721 However, protective effects of metformin against the radiation mimetic doxorubicin were only
722 observed at low concentrations due to the suppression of platelet-derived growth factor receptor
723 (PDGFR) expression by high metformin (Kobashigawa, Xu, Padbury, Tseng, & Yano, 2014). In vivo,
724 high metformin doses shortened the lifespan of mice (Palliyaguru et al., 2020). Other receptor
725 tyrosine kinases including FGFR1 have also been involved in the cellular responses to metformin (Shi
726 et al., 2021). In low concentrations, metformin was able to suppress oxidative stress-associated
727 senescence of adipose-derived stromal cells via activation of AMPK, but it is unclear whether this
728 was NOX-dependent (Le Pelletier et al., 2021). A more detailed analysis of the network of signaling
729 pathways mediating NOX4 suppression by low metformin is clearly warranted but remains outside
730 the scope of the present study.

731 Our study has a number of limitations. Whole body irradiation is an over-simplified model for
732 therapeutic irradiation of tumour patients. However, experiments with localised radiation to the
733 brain have also shown improvements in cognition immediately after senolytic intervention
734 (Yabluchanskiy et al., 2020). Moreover, senolytic intervention with D+Q after irradiation targeted to
735 a single leg resulted in long-term improvements of muscle function (Zhu et al., 2015). These,
736 together with our results, strongly suggest that senolytic or senostatic interventions could be
737 effective against progressive frailty, multimorbidity and mortality even in realistic radiation therapy
738 situations. We have now established a more realistic mouse model for targeted brain tumour
739 radiation therapy. Pilot phenotyping results show progressive frailty development together with

740 cognitive decline not dissimilar to the effects of whole-body irradiation, and results of an
741 intervention study will be published as soon as possible.

742 Lifespan-extending interventions frequently show strong sexual dimorphism (Nadon, Strong, Miller,
743 & Harrison, 2017). It is therefore important to test the impact of senolytic/senostatic interventions
744 post-irradiation in both males and females. This could not be done in the present cohorts due to
745 funding restrictions. However, independent validation cohorts have been set up using the same
746 protocols and show significant improvements in frailty in irradiated females as well, following
747 senolytic interventions (M. Weigand et al., in preparation).

748 In conclusion, we have shown that short senolytic or senostatic interventions can effectively rescue
749 premature progressive frailty and accelerated ageing induced by whole body irradiation over a
750 significant part of the life history in male mice. We believe these results warrant further efforts to
751 translate senolytic and senostatic interventions towards an adjuvant therapy for long-term tumour
752 survivors.

753

754

755 **Acknowledgements**

756 This study was supported by Cancer Research UK (www.cancerresearchuk.org) Pioneer Award
757 C12161/A24009 and P&G/BBSRC (www.bbsrc.ukri.org) grant BB/S006710/1 to TvZ, an MRC –
758 Arthritis Research UK, Centre for Integrated Research into Musculoskeletal Ageing
759 (www.cimauk.org) Translation grant and UK SPINE Bridge (www.kespine.org.uk) grant B06 to SM and
760 TvZ, a P&G/BBSRC DTP (www.bbsrc.ukri.org/skills/investing-doctoral-training/dtp) studentship
761 (BH174490) to VIK and a BBSRC DTP (www.bbsrc.ukri.org/skills/investing-doctoral-training/dtp)
762 studentship to DJ. The funders had no role in study design, data collection and analysis, decision to
763 publish, or preparation of the manuscript. We thank the Comparative Biology Centre at Newcastle
764 University, in particular Mr. Christopher Huggins, for their expert support with animal husbandry,
765 Drs Andrew Filby and David McDonald at Flow Cytometry Core Facility, Newcastle University for
766 their expert support with CyTOF experiments, and Dr I Karakesisoglou and Dr P Chazot, Durham
767 University, for their support in early supervision of MW.

768 Author contributions: EF, TW, GA, AI, EL, MW (under supervision by DJ), GK (under supervision by
769 VIK), CP, BG and SM performed experiments, TvZ and SM designed and supervised the study, EF, DJ,
770 VIK, SM and TvZ wrote the paper. All authors agreed with the submitted version.

771 The authors have no competing interests to declare.

772

773 **References:**

774 Aravinthan, A. D., & Alexander, G. J. M. (2016). Senescence in chronic liver disease: Is the future in
775 aging? *J Hepatol*, 65(4), 825-834.

776 Baar, M. P., Brandt, R. M., Putavet, D. A., Klein, J. D., Derk, K. W., Bourgeois, B. R., et al. (2017).
777 Targeted Apoptosis of Senescent Cells Restores Tissue Homeostasis in Response to
778 Chemotoxicity and Aging. *Cell*, 169(1), 132-147 e116.

779 Birket, M. J., Orr, A. L., Gerencser, A. A., Madden, D. T., Vitelli, C., Swistowski, A., et al. (2011). A
780 reduction in ATP demand and mitochondrial activity with neural differentiation of human
781 embryonic stem cells. *J Cell Sci*, 124(Pt 3), 348-358.

782 Blagosklonny, M. V. (2017). From rapalogs to anti-aging formula. *Oncotarget*, 8(22), 35492-35507.

783 Bluethmann, S. M., Mariotto, A. B., & Rowland, J. H. (2016). Anticipating the "Silver Tsunami":
784 Prevalence Trajectories and Comorbidity Burden among Older Cancer Survivors in the
785 United States. *Cancer epidemiology, biomarkers & prevention : a publication of the American
786 Association for Cancer Research, cosponsored by the American Society of Preventive
787 Oncology*, 25(7), 1029-1036.

788 Brand, M. D. (2005). The efficiency and plasticity of mitochondrial energy transduction. *Biochem Soc
789 Trans*, 33(Pt 5), 897-904.

790 Bray, F., Ferlay, J., Soerjomataram, I., Siegel, R. L., Torre, L. A., & Jemal, A. (2018). Global cancer
791 statistics 2018: GLOBOCAN estimates of incidence and mortality worldwide for 36 cancers in
792 185 countries. *CA Cancer J Clin*, 68(6), 394-424.

793 Cameron, K. M., Miwa, S., Walker, C., & von Zglinicki, T. (2012). Male mice retain a metabolic
794 memory of improved glucose tolerance induced during adult onset, short-term dietary
795 restriction. *Longev Healthspan*, 1, 3.

796 Campbell, J. M., Bellman, S. M., Stephenson, M. D., & Lisy, K. (2017). Metformin reduces all-cause
797 mortality and diseases of ageing independent of its effect on diabetes control: A systematic
798 review and meta-analysis. *Ageing Res Rev*, 40, 31-44.

799 Chandra, A., Lagnado, A. B., Farr, J. N., Monroe, D. G., Park, S., Hachfeld, C., et al. (2020). Targeted
800 Reduction of Senescent Cell Burden Alleviates Focal Radiotherapy-Related Bone Loss. *J Bone
801 Miner Res*, 35(6), 1119-1131.

802 Chang, J., Wang, Y., Shao, L., Laberge, R. M., Demaria, M., Campisi, J., et al. (2016). Clearance of
803 senescent cells by ABT263 rejuvenates aged hematopoietic stem cells in mice. *Nat Med*,
804 22(1), 78-83.

805 Coppe, J. P., Desprez, P. Y., Krtolica, A., & Campisi, J. (2010). The senescence-associated secretory
806 phenotype: the dark side of tumor suppression. *Annu Rev Pathol*, 5, 99-118.

807 Cupit-Link, M. C., Kirkland, J. L., Ness, K. K., Armstrong, G. T., Tchkonia, T., LeBrasseur, N. K., et al.
808 (2017). Biology of premature ageing in survivors of cancer. *ESMO Open*, 2(5), e000250.

809 Cytlak, U., Resteu, A., Pagan, S., Green, K., Milne, P., Maisuria, S., et al. (2020). Differential IRF8
810 Transcription Factor Requirement Defines Two Pathways of Dendritic Cell Development in
811 Humans. *Immunity*, 53(2), 353-370 e358.

812 da Silva, P. F. L., Ogrodnik, M., Kucheryavenko, O., Glibert, J., Miwa, S., Cameron, C., et al. (2019).
813 The bystander effect contributes to the accumulation of senescent cells in vivo. *Aging Cell*,
814 18, e12848.

815 Dalle Pezze, P., Nelson, G., Otten, E. G., Korolchuk, V. I., Kirkwood, T. B., von Zglinicki, T., et al.
816 (2014). Dynamic modelling of pathways to cellular senescence reveals strategies for targeted
817 interventions. *PLoS Comput Biol*, 10(8), e1003728.

818 Damlaj, M., El Fakih, R., & Hashmi, S. K. (2019). Evolution of survivorship in lymphoma, myeloma and
819 leukemia: Metamorphosis of the field into long term follow-up care. *Blood Rev*, 33, 63-73.

820 Davalos, A. R., Kawahara, M., Malhotra, G. K., Schaum, N., Huang, J., Ved, U., et al. (2013). p53-
821 dependent release of Alarmin HMGB1 is a central mediator of senescent phenotypes. *J Cell
822 Biol*, 201(4), 613-629.

823 Demaria, M. (2017). Senescent cells: New target for an old treatment? *Mol Cell Oncol*, 4(3),
824 e1299666.

825 Demaria, M., O'Leary, M. N., Chang, J., Shao, L., Liu, S., Alimirah, F., et al. (2017). Cellular Senescence
826 Promotes Adverse Effects of Chemotherapy and Cancer Relapse. *Cancer Discov*, 7(2), 165-
827 176.

828 Fielder, E., Tweedy, C., Wilson, C., Oakley, F., LeBeau, F. E. N., Passos, J. F., et al. (2020). Anti-
829 inflammatory treatment rescues memory deficits during aging in nfkb1(-/-) mice. *Aging Cell*,
830 19(10), e13188.

831 Fielder, E., Weigand, M., Agneessens, J., Griffin, B., Parker, C., Miwa, S., et al. (2019). Sublethal
832 whole-body irradiation causes progressive premature frailty in mice. *Mech Ageing Dev*, 180,
833 63-69.

834 Fontana, L., Nehme, J., & Demaria, M. (2018). Caloric restriction and cellular senescence. *Mech
835 Ageing Dev*, 176, 19-23.

836 Gorgoulis, V. G., Adams, P. D., Alimonti, A., Bennett, D. C., Bischof, O., Bishop, C., et al.
837 (2019). Cellular Senescence: Defining a path forward. *Cell*, 179, 813-827.

838 Goy, C., Czypiorski, P., Altschmied, J., Jakob, S., Rabanter, L. L., Brewer, A. C., et al. (2014). The
839 imbalanced redox status in senescent endothelial cells is due to dysregulated Thioredoxin-1
840 and NADPH oxidase 4. *Exp Gerontol*, 56, 45-52.

841 Hewitt, G., Jurk, D., Marques, F. D., Correia-Melo, C., Hardy, T., Gackowska, A., et al. (2012).
842 Telomeres are favoured targets of a persistent DNA damage response in ageing and stress-
843 induced senescence. *Nat Commun*, 3, 708.

844 Hudgins, A. D., Tazearslan, C., Tare, A., Zhu, Y., Huffman, D., & Suh, Y. (2018). Age- and Tissue-
845 Specific Expression of Senescence Biomarkers in Mice. *Front Genet*, 9, 59.

846 Jena, B. C., Das, C. K., Bharadwaj, D., & Mandal, M. (2020). Cancer associated fibroblast mediated
847 chemoresistance: A paradigm shift in understanding the mechanism of tumor progression.
848 *Biochim Biophys Acta Rev Cancer*, 1874(2), 188416.

849 Jurk, D., Wilson, C., Passos, J. F., Oakley, F., Correia-Melo, C., Greaves, L., et al. (2014). Chronic
850 inflammation induces telomere dysfunction and accelerates ageing in mice. *Nat Commun*, 2,
851 4172.

852 Katayama, H., Kogure, T., Mizushima, N., Yoshimori, T., & Miyawaki, A. (2011). A sensitive and
853 quantitative technique for detecting autophagic events based on lysosomal delivery. *Chem
854 Biol*, 18(8), 1042-1052.

855 Kilkenny, C., Browne, W. J., Cuthill, I. C., Emerson, M., & Altman, D. G. (2010). Improving bioscience
856 research reporting: the ARRIVE guidelines for reporting animal research. *PLoS Biol*, 8(6),
857 e1000412.

858 Kobashigawa, L. C., Xu, Y. C., Padbury, J. F., Tseng, Y. T., & Yano, N. (2014). Metformin protects
859 cardiomyocyte from doxorubicin induced cytotoxicity through an AMP-activated protein
860 kinase dependent signaling pathway: an in vitro study. *PLoS One*, 9(8), e104888.

861 Kojima, G., Iliffe, S., & Walters, K. (2018). Frailty index as a predictor of mortality: a systematic
862 review and meta-analysis. *Age Ageing*, 47(2), 193-200.

863 Korolchuk, V. I., Miwa, S., Carroll, B., & von Zglinicki, T. (2017). Mitochondria in Cell Senescence: Is
864 Mitophagy the Weakest Link? *EBioMedicine*, 21, 7-13.

865 Lazarou, M., Sliter, D. A., Kane, L. A., Sarraf, S. A., Wang, C., Burman, J. L., et al. (2015). The ubiquitin
866 kinase PINK1 recruits autophagy receptors to induce mitophagy. *Nature*, 524(7565), 309-
867 314.

868 Le, O. N., Rodier, F., Fontaine, F., Coppe, J. P., Campisi, J., DeGregori, J., et al. (2010). Ionizing
869 radiation-induced long-term expression of senescence markers in mice is independent of
870 p53 and immune status. *Aging Cell*, 9(3), 398-409.

871 Le Pelletier, L., Mantecon, M., Gorwood, J., Auclair, M., Foresti, R., Motterlini, R., et al. (2021).
872 Metformin alleviates stress-induced cellular senescence of aging human adipose stromal
873 cells and the ensuing adipocyte dysfunction. *Elife*, 10.

874 Lener, B., Koziel, R., Pircher, H., Hutter, E., Greussing, R., Herndler-Brandstetter, D., et al. (2009). The
875 NADPH oxidase Nox4 restricts the replicative lifespan of human endothelial cells. *Biochem J*,
876 423(3), 363-374.

877 Lopez-Otin, C., Galluzzi, L., Freije, J. M. P., Madeo, F., & Kroemer, G. (2016). Metabolic Control of
878 Longevity. *Cell*, 166(4), 802-821.

879 Martin-Montalvo, A., Mercken, E. M., Mitchell, S. J., Palacios, H. H., Mote, P. L., Scheibye-Knudsen,
880 M., et al. (2013). Metformin improves healthspan and lifespan in mice. *Nat Commun*, 4,
881 2192.

882 Miwa, S., Jow, H., Baty, K., Johnson, A., Czapiewski, R., Saretzki, G., et al. (2014). Low abundance of
883 the matrix arm of complex I in mitochondria predicts longevity in mice. *Nat Commun*, 5,
884 3837.

885 Miwa, S., Treumann, A., Bell, A., Vistoli, G., Nelson, G., Hay, S., et al. (2016). Carboxylesterase
886 converts Amplex red to resorufin: Implications for mitochondrial H₂O₂ release assays. *Free
887 Radic Biol Med*, 90, 173-183.

888 Moiseeva, O., Deschenes-Simard, X., St-Germain, E., Igelmann, S., Huot, G., Cedar, A. E., et al. (2013).
889 Metformin inhibits the senescence-associated secretory phenotype by interfering with
890 IKK/NF-kappaB activation. *Aging Cell*, 12(3), 489-498.

891 Mookerjee, S. A., & Brand, M. D. (2015). Measurement and Analysis of Extracellular Acid Production
892 to Determine Glycolytic Rate. *J Vis Exp*(106), e53464.

893 Musi, N., Valentine, J. M., Sickora, K. R., Baeuerle, E., Thompson, C. S., Shen, Q., et al. (2018). Tau
894 protein aggregation is associated with cellular senescence in the brain. *Aging Cell*, 17(6),
895 e12840.

896 Mylonas, K. J., O'Sullivan, E. D., Humphries, D., Baird, D. P., Docherty, M. H., Neely, S. A., et al.
897 (2021). Cellular senescence inhibits renal regeneration after injury in mice, with senolytic
898 treatment promoting repair. *Sci Transl Med*, 13(594).

899 Nadon, N. L., Strong, R., Miller, R. A., & Harrison, D. E. (2017). NIA Interventions Testing Program:
900 Investigating Putative Aging Intervention Agents in a Genetically Heterogeneous Mouse
901 Model. *EBioMedicine*, 21, 3-4.

902 Nelson, G., Kucheryavko, O., Wordsworth, J., & von Zglinicki, T. (2018). The senescent bystander
903 effect is caused by ROS-activated NF-kappaB signalling. *Mech Ageing Dev*, 170, 30-36.

904 Nelson, G., Wordsworth, J., Wang, C., Jurk, D., Lawless, C., Martin-Ruiz, C., et al. (2012). A senescent
905 cell bystander effect: senescence-induced senescence. *Aging Cell*, 11(2), 345-349.

906 Ness, K. K., Kirkland, J. L., Gramatges, M. M., Wang, Z., Kundu, M., McCastlain, K., et al. (2018).
907 Premature Physiologic Aging as a Paradigm for Understanding Increased Risk of Adverse
908 Health Across the Lifespan of Survivors of Childhood Cancer. *J Clin Oncol*, 36(21), 2206-2215.

909 Ness, K. K., Krull, K. R., Jones, K. E., Mulrooney, D. A., Armstrong, G. T., Green, D. M., et al. (2013).
910 Physiologic frailty as a sign of accelerated aging among adult survivors of childhood cancer: a
911 report from the St Jude Lifetime cohort study. *J Clin Oncol*, 31(36), 4496-4503.

912 Ogorodnik, M., Evans, S. A., Fielder, E., Victorelli, S., Kruger, P., Salmonowicz, H., et al. (2021). Whole-
913 body senescent cell clearance alleviates age-related brain inflammation and cognitive
914 impairment in mice. *Aging Cell*, 20(2), e13296.

915 Ogorodnik, M., Miwa, S., Tchkonia, T., Tiniakos, D., Wilson, C. L., Lahat, A., et al. (2017). Cellular
916 senescence drives age-dependent hepatic steatosis. *Nat Commun*, 8, 15691.

917 Palacio, L., Goyer, M. L., Maggiorani, D., Espinosa, A., Villeneuve, N., Bourbonnais, S., et al. (2019).
918 Restored immune cell functions upon clearance of senescence in the irradiated splenic
919 environment. *Aging Cell*, 18(4), e12971.

920 Palacio, L., Krishnan, V., Le, N. L., Sharpless, N. E., & Beausejour, C. M. (2017). Sustained p16(INK4a)
921 expression is required to prevent IR-induced tumorigenesis in mice. *Oncogene*, 36(9), 1309-
922 1314.

923 Palliyaguru, D. L., Minor, R. K., Mitchell, S. J., Palacios, H. H., Licata, J. J., Ward, T. M., et al. (2020).
924 Combining a High Dose of Metformin With the SIRT1 Activator, SRT1720, Reduces Life Span
925 in Aged Mice Fed a High-Fat Diet. *J Gerontol A Biol Sci Med Sci*, 75(11), 2037-2041.

926 Passos, J. F., Nelson, G., Wang, C., Richter, T., Simillion, C., Proctor, C. J., et al. (2010). Feedback
927 between p21 and reactive oxygen production is necessary for cell senescence. *Mol Syst Biol*,
928 6, 347.

929 Passos, J. F., Saretzki, G., Ahmed, S., Nelson, G., Richter, T., Peters, H., et al. (2007). Mitochondrial
930 dysfunction accounts for the stochastic heterogeneity in telomere-dependent senescence.
931 *PLoS Biol*, 5(5), e110.

932 Rezende, F., Schurmann, C., Schutz, S., Harenkamp, S., Herrmann, E., Seimetz, M., et al. (2017).
933 Knock out of the NADPH oxidase Nox4 has no impact on life span in mice. *Redox Biol*, 11,
934 312-314.

935 Robison, L. L., & Hudson, M. M. (2014). Survivors of childhood and adolescent cancer: life-long risks
936 and responsibilities. *Nat Rev Cancer*, 14(1), 61-70.

937 Rockwood, K., Mitnitski, A., & Howlett, S. E. (2015). Frailty: Scaling from Cellular Deficit
938 Accumulation? *Interdiscip Top Gerontol Geriatr*, 41, 1-14.

939 Saleh, T., Tyutyunyk-Massey, L., & Gewirtz, D. A. (2019). Tumor Cell Escape from Therapy-Induced
940 Senescence as a Model of Disease Recurrence after Dormancy. *Cancer Res*, 79(6), 1044-
941 1046.

942 Sato, N., Takasaka, N., Yoshida, M., Tsubouchi, K., Minagawa, S., Araya, J., et al. (2016). Metformin
943 attenuates lung fibrosis development via NOX4 suppression. *Respir Res*, 17(1), 107.

944 Selvarani, R., Mohammed, S., & Richardson, A. (2021). Effect of rapamycin on aging and age-related
945 diseases-past and future. *Geroscience*, 43(3), 1135-1158.

946 Seol, M. A., Jung, U., Eom, H. S., Kim, S. H., Park, H. R., & Jo, S. K. (2012). Prolonged expression of
947 senescence markers in mice exposed to gamma-irradiation. *J Vet Sci*, 13(4), 331-338.

948 Shi, Y., & Hou, S. A. (2021). Protective effects of metformin against myocardial ischemiareperfusion
949 injury via AMPKdependent suppression of NOX4. *Mol Med Rep*, 24(4).

950 Shi, Y., Ma, Z., Cheng, Q., Wu, Y., Parris, A. B., Kong, L., et al. (2021). FGFR1 overexpression renders
951 breast cancer cells resistant to metformin through activation of IRS1/ERK signaling. *Biochim
952 Biophys Acta Mol Cell Res*, 1868(1), 118877.

953 Short, S., Fielder, E., Miwa, S., & von Zglinicki, T. (2019). Senolytics and senostatics as adjuvant
954 tumour therapy. *EBioMedicine*, 41, 683-692.

955 te Poele, R. H., Okorokov, A. L., Jardine, L., Cummings, J., & Joel, S. P. (2002). DNA damage is able to
956 induce senescence in tumor cells in vitro and in vivo. *Cancer Res*, 62(6), 1876-1883.

957 von Zglinicki, T. (2021). Mechanisms of cell senescence in aging. In N. Musi & P. Hornsby (Eds.),
958 *Handbook of the Biology of Aging* (9th ed., pp. 53-68): Academic Press.

959 Wang, C., Maddick, M., Miwa, S., Jurk, D., Czapiewski, R., Saretzki, G., et al. (2010). Adult-onset,
960 short-term dietary restriction reduces cell senescence in mice. *Aging (Albany NY)*, 2(9), 555-
961 566.

962 Wang, C. P., Lorenzo, C., Habib, S. L., Jo, B., & Espinoza, S. E. (2017). Differential effects of metformin
963 on age related comorbidities in older men with type 2 diabetes. *J Diabetes Complications*,
964 31(4), 679-686.

965 Weyemi, U., Lagente-Chevallier, O., Boufraqech, M., Prenois, F., Courtin, F., Caillou, B., et al. (2012).
966 ROS-generating NADPH oxidase NOX4 is a critical mediator in oncogenic H-Ras-induced DNA
967 damage and subsequent senescence. *Oncogene*, 31(9), 1117-1129.

968 Whitehead, J. C., Hildebrand, B. A., Sun, M., Rockwood, M. R., Rose, R. A., Rockwood, K., et al.
969 (2014). A clinical frailty index in aging mice: comparisons with frailty index data in humans. *J
970 Gerontol A Biol Sci Med Sci*, 69(6), 621-632.

971 Wilcock, C., & Bailey, C. J. (1994). Accumulation of metformin by tissues of the normal and diabetic
972 mouse. *Xenobiotica*, 24(1), 49-57.

973 Xu, M., Pirtskhalava, T., Farr, J. N., Weigand, B. M., Palmer, A. K., Weivoda, M. M., et al. (2018).
974 Senolytics improve physical function and increase lifespan in old age. *Nat Med*, doi:
975 10.1038/s41591-41018-40092-41599.
976 Yabluchanskiy, A., Tarantini, S., Balasubramanian, P., Kiss, T., Csipo, T., Fulop, G. A., et al. (2020).
977 Pharmacological or genetic depletion of senescent astrocytes prevents whole brain
978 irradiation-induced impairment of neurovascular coupling responses protecting cognitive
979 function in mice. *Geroscience*, 42(2), 409-428.
980 Zhu, Y., Tchkonia, T., Fuhrmann-Stroissnigg, H., Dai, H. M., Ling, Y. Y., Stout, M. B., et al. (2016).
981 Identification of a novel senolytic agent, navitoclax, targeting the Bcl-2 family of anti-
982 apoptotic factors. *Aging Cell*, 15(3), 428-435.
983 Zhu, Y., Tchkonia, T., Pirtskhalava, T., Gower, A. C., Ding, H., Giorgadze, N., et al. (2015). The Achilles'
984 heel of senescent cells: from transcriptome to senolytic drugs. *Aging Cell*, 14(4), 644-658.
985 Zou, Y., Sfeir, A., Gryaznov, S. M., Shay, J. W., & Wright, W. E. (2004). Does a sentinel or a subset of
986 short telomeres determine replicative senescence? *Mol Biol Cell*, 15(8), 3709-3718.
987
988
989

990 **Tables**

991

992 **Table 1: Immunostaining and blotting methods**

Tissue	Thickness	Technique	Primary antibody	Cat No, vendor	Dilution	Secondary antibody	Cat No, vendor	Dilution	Detection
Liver	3	IF	Rabbit anti-HMGB1	Ab7982 3 (Abcam)	1:250	Goat Anti-Rabbit IgG H&L, Texas Red	Ab6719 (Abcam)	1:500	
	3	IF	Mouse anti-TOMM20	Ab5678 3 (Abcam)	1:200	Goat anti-mouse (Alexa Fluor 594)	Ab1501 16	1:1000	
Quads	3	IF	Rabbit anti-HMGB1	Ab7982 3 (Abcam)	1:250	Goat anti-rabbit (Alexa Fluor 594)	A32740 (Thermo Fisher)	1:1000	
Brain	10	IHC	Rabbit anti-Iba1	Ab1788 46 (Abcam)	1:2000	Biotinylated Goat anti-rabbit	BA-1000 (Vector labs)	1:250	VECTASTAIN ABC-HRP Kit, NovaRED (Vector labs)
	3	IF	Rabbit anti- γ H2A.X primary antibody	9718 (Cell Signalling)	1:250	Biotinylated Goat anti-rabbit	BA-1000 (Vector labs)	1:250	Fluorescein Avidin DCS (1:500) (Vector labs)
	3	IF	Rabbit anti-Lamin B1	ab1604 8 (Abcam)	1:200	Biotinylated Goat anti-rabbit	BA-1000 (Vector labs)	1:250	Fluorescein Avidin DCS (1:500) (Vector labs)
MRC5 Cells	ICC		Anti-NADPH oxidase 4 antibody	ab1092 25 (Abcam)	1:200	Goat Anti-Rabbit IgG H&L (Alexa Fluor [®] 594)	ab1500 80 (Abcam)	1:1000	
			Anti-IL6 antibody	ab9324 (Abcam)	1:500	Anti-Mouse IgG (H+L) Alexa Fluor 488	A-11017 (vector labs)	1:1000	
			Rabbit anti-p21	ab1095 20 (Abcam)	1:100	Goat Anti-Rabbit IgG H&L (Alexa Fluor [®] 594)	ab1500 80 (Abcam)	1:1000	

		Rabbit anti-HMGB1	ab79823 (Abcam)	1:250	Goat Anti-Rabbit IgG H&L (Alexa Fluor® 594)	ab150080 (Abcam)	1:1000	
Protein	WB	Anti-NADPH oxidase 4 antibody	ab109225 (Abcam)	1:2000	Goat Anti-Rabbit IgG H&L (HRP)	ab6721 (Abcam)	1:10000	
		Anti-β-Actin antibody	5125 (Cell Signaling)	1:1000	Goat Anti-Rabbit IgG H&L (HRP)	ab6721 (Abcam)	1:10000	

993

994 **Table 2. List of metal conjugated antibodies for stress response pathway analysis by CyTOF**

Antibody	Metal	cat #	Vendor
SOD2/MnSOD [9E2BD2]	176Yb	ab110300	Abcam
GSTM2 (9E975)	167Er	H00002946-M03	Novus Biologicals
HSF1	153Eu	825801	BioLegend
Hsp-70 (2A4)	154Sm	ab5442	Abcam
Nrf2 (phospho S40) [EP1809Y]	142Nd	ab180844	Abcam
NR1L2/PXR (6H11D8)	164Dy	LS-C682408-LSP	Stratech Scientific Ltd.
GRP78 BiP [EPR4041(2)]	161Dy	ab108615	Abcam
EIF2S1 (phospho S51) (E90)	169Tm	ab214434	Abcam
ATF-6 (-Carboxy terminal end)	175Lu	ab62576	Abcam
GADD153/CHOP	141Pr	NBP2-13172	Novus Biologicals
CLPP [EPR7133]	165Ho	ab236064	Abcam
Hsp-60 (LK1)	144Nd	ab212454	Abcam
pS6 [S235/S236]	172Yb	3172008A	Fluidigm
p21 Waf1/Cip1	159Tb	3159026A	Fluidigm
Phospho-Acetyl-CoA Carboxylase (Ser79) (10HCLC)	170Er	711289	ThermoFisher
p62 / SQSTM1 (C-terminus)	146Nd	GP62-C	Progen
p-p38 [T180/Y182]	156Gd	3156002A	Fluidigm
DNA/RNA damage	173Yb	ab62623	Abcam
pHistone H2A.X [Ser139]	147Sm	NB100-384	Novus Biologicals
PHB	151Eu	NBP2-32305	Novus Biologicals
p16INK4	174Yb	ab54210	Abcam
Cell-ID™ Intercalator-Ir—500μM		201192B	Fluidigm

995

996

997 **List of Supplementary Materials:**

998 • Figure 1-figure supplement 1. Components of the frailty index (FI).

999 • Figure 1-figure supplement 2. Impact of interventions on epidermal thickness.

1000 • Figure 1-figure supplement 3. Validation of senescence markers in liver.

1001 • Figure 1-figure supplement 4. Impact of early senolytics treatment on hepatocyte

1002 senescence at late age.

1003 • Figure 1-figure supplement 5. Senescence and neuroinflammation markers in hippocampus

1004 after early senolytic intervention.

1005 • Figure 1-figure supplement 6. Functional and senescence markers in skeletal muscle after

1006 early intervention with D+Q or Navitoclax.

1007 • Figure 2-figure supplement 1. Late intervention with either D+Q or Navitoclax (at 12

1008 months of age) does not change epithelial thickness at 16 months.

1009 • Figure 2-figure supplement 2. Impact of late senolytics treatment on senescence markers in

1010 liver.

1011 • Figure 2-figure supplement 3. Functional and senescence markers in skeletal muscle after

1012 late intervention with D+Q or Navitoclax.

1013 • Figure 2-figure supplement 4. Impact of late intervention on neuroinflammation.

1014 • Figure 3 – Figure supplement 1. Treatment of irradiated mice for 2.5 months with metformin

1015 (starting at 7 months of age) tends to reduce epidermal thickness at late age (16 months).

1016 • Figure 3 – Figure supplement 2. Impact of metformin on senescence markers in liver.

1017 • Figure 3 – Figure supplement 3. Senescence and neuroinflammation markers in

1018 hippocampus after intervention with metformin.

1019 • Figure 3 – Figure supplement 4. Impact of metformin on hind limb muscle.

1020 • Figure 5 – Figure supplement 1. Representative histogram overlay examples for use of

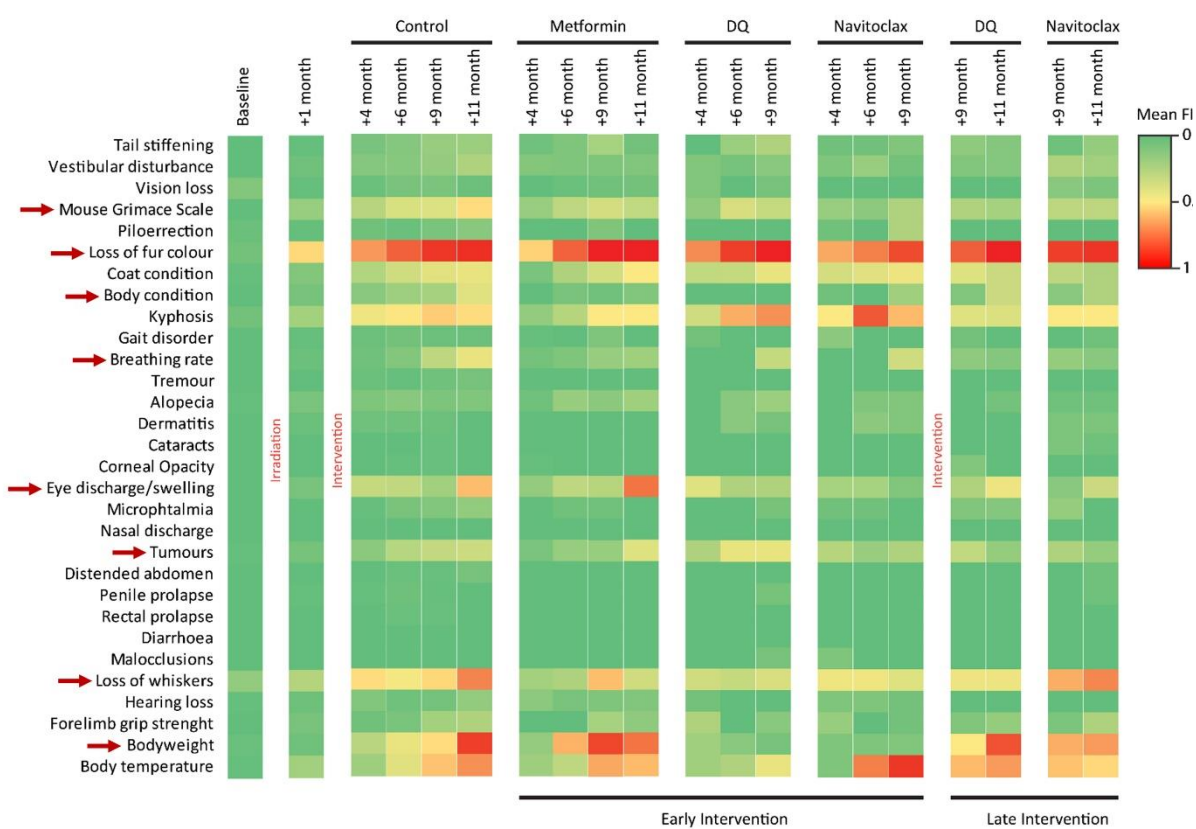
1021 CyTOF as stress pathway identifier.

1022 • Figure 6 – supplement 1. NOX4 does not co-localise with mitochondria.

1023

1024 **Supplementary Figures**

1025



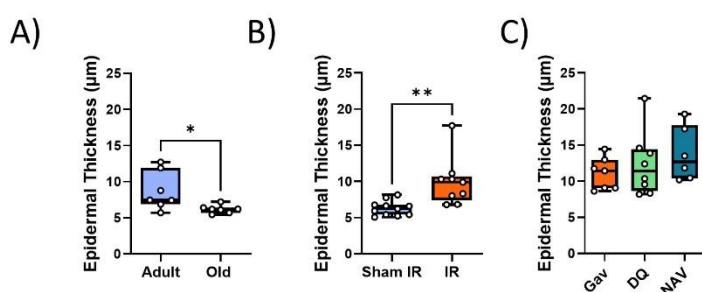
1026

1027

1028 **Figure 1-Figure supplement 1. Components of the frailty index (FI).** Colours represent the mean FI
1029 of all animals alive at that given point (8 – 12 animals/group). Red arrows indicate components that
1030 were improved under the interventions.

1031

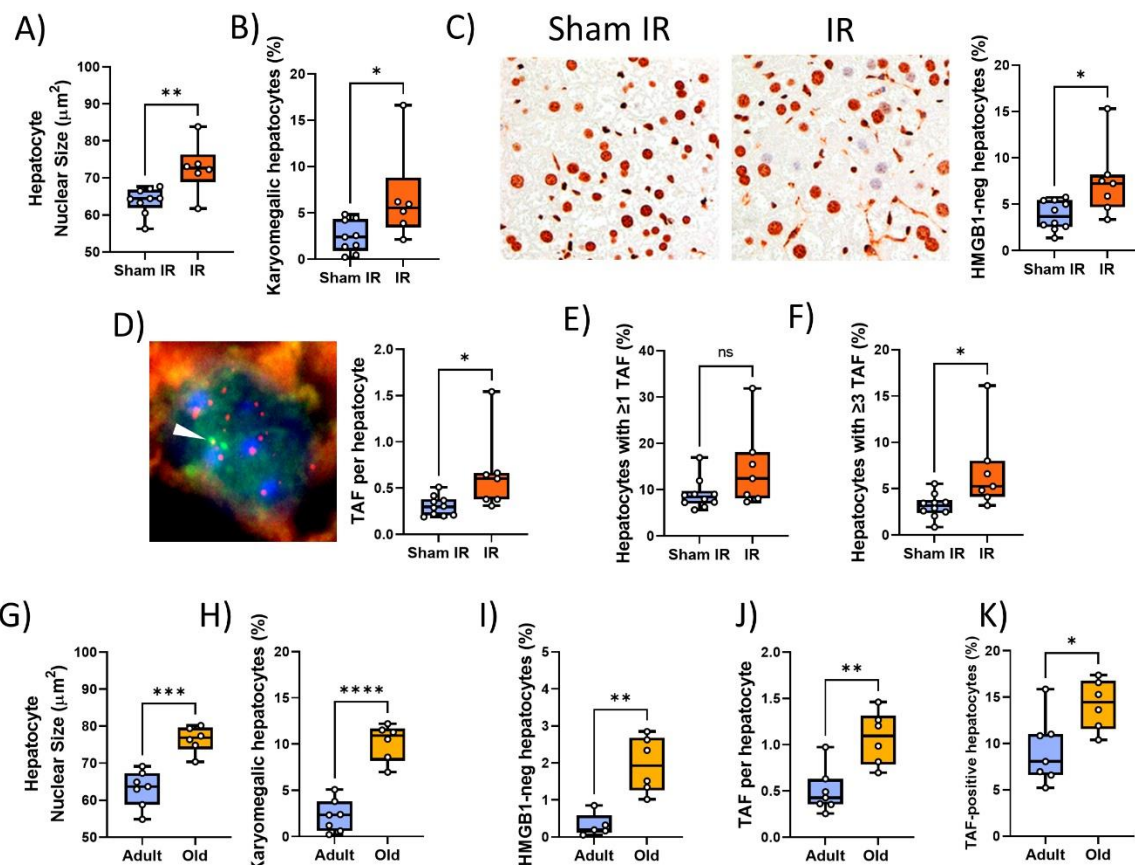
1032



1033

1034 **Figure 1 – Figure supplement 2. Impact of interventions on epidermal thickness.** A) Epidermal
1035 thickness decreases in old (median age 32months) as compared to young adult (median age 10
1036 months) mice. B) IR at 5 months of age results in increased epidermal thickness at 12 months. C)
1037 Treatment of irradiated mice with senolytics D+Q or Navitoclax at 7 months of age does not change
1038 epidermal thickness at 16 months of age. Data are from at least 7 animals/group.

1039

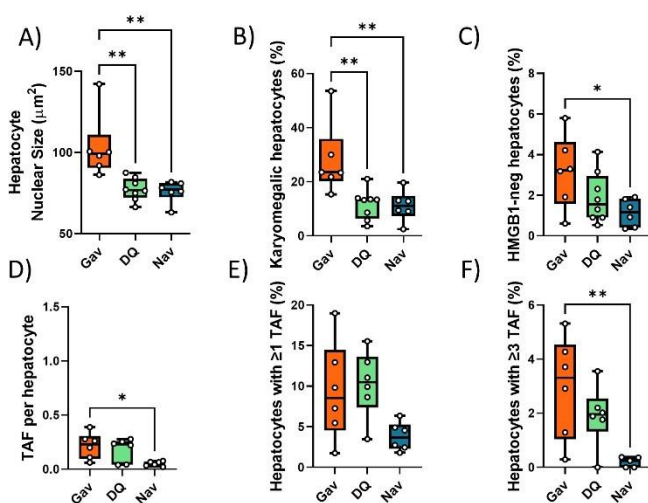


1040

1041 **Figure 1-figure supplement 3. Validation of senescence markers in liver.** (A-F) Irradiated vs sham-
1042 irradiated mice at 12 months of age. A) nuclear area, B) Frequency of karyomegalic hepatocytes. C)
1043 HMGB1 immunohistochemistry. Left: representative HMGB1 micrographs (left: control, right:
1044 7months past IR). Right: Frequencies of HMGB1-negative hepatocytes. D) TAF assay. Left:
1045 Representative TAF immunoFISH image (single focal plane, arrowhead indicates overlap of a
1046 telomere (red) with a γ H2AX focus (green), e.g. TAF). Right: Average TAF frequency per hepatocyte
1047 nucleus. E) Frequency of TAF-positive hepatocytes. F) Frequency of hepatocytes with at least 3 TAF.
1048 (G-K) Young adult (8-14 months) vs old (32 months) mice. Nuclear area (G), frequencies of
1049 karyomegalic hepatocytes (H), frequencies of HMGB1-negative hepatocytes (I), TAF frequency per
1050 nucleus (J) and Frequency of hepatocytes with at least 1 TAF (K). Data are from at least 6
1051 animals/group.

1052

1053



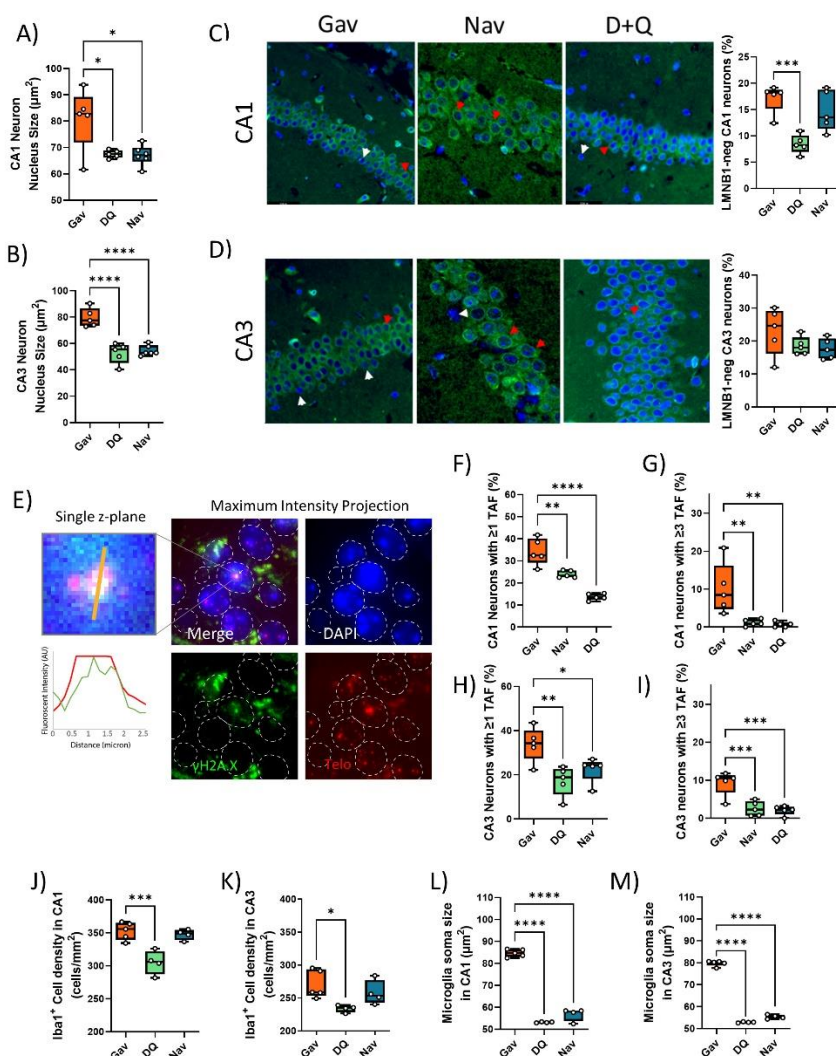
1054

1055

1056 **Figure 1-figure supplement 4. Impact of early senolytics treatment on hepatocyte senescence at**
1057 **late age (16 months). Nuclear size (A), percentage of karyomegalic hepatocytes (B), percentage of**
1058 **HMGB1-negative hepatocytes (C), TAF frequency per nucleus (D), frequency of TAF-positive cells (E)**
1059 **and frequency of cells with at least 3 TAF (F) in mice livers at 16 months of age, irradiated at 5**
1060 **months and treated with either D+Q, Navitoclax or sham gavage at 6 months. Data are from at least**
1061 **6 animals/group.**

1062

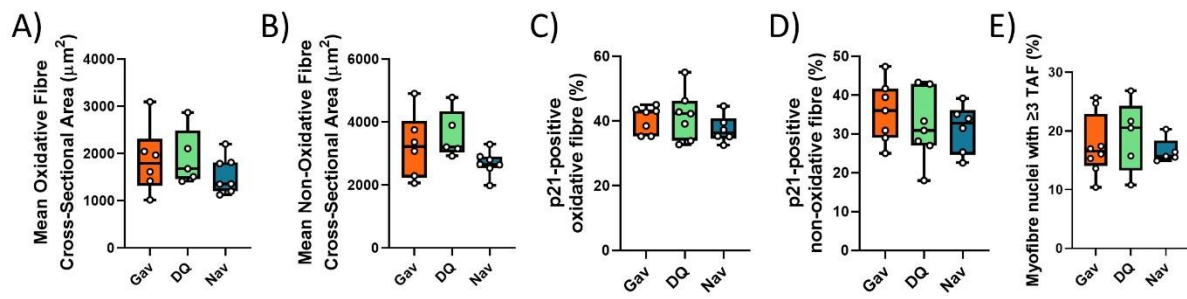
1063



1064

1065 **Figure 1 – figure supplement 5. Senescence and neuroinflammation markers in hippocampus after**
1066 **early senolytic intervention.** Neuron nuclear area in CA1 (A) and CA3 (B). C,D) Left: LaminB1
1067 Immunostaining (green) in CA1 (C) and CA3 (D) regions of the hippocampus under the different
1068 treatments. Blue: DAPI. Arrowheads indicate Lmn1-positive (red) and –negative (white) nuclei.
1069 Right: Frequencies of laminB1-negative neurons in CA1 (top) and CA3 (bottom). E) TAF ImmunoFISH
1070 of neurons in the CA1 area. Left: Higher magnification of a single TAF (single plane image) and
1071 intensity scans for green (gH2AX) and red (telomere) fluorescence. Right: Maximum intensity
1072 projections. Frequencies of TAF-positive neurons in CA1 (F) and CA3 (H). Frequencies of neurons
1073 with at least 3 TAF in CA1 (G) and CA3 (I). Iba1+ cell density in CA1 (J) and CA3 (K). Iba1+ cell soma
1074 size in CA1 (L) and CA3 (M). Data are from at least 6 animals/group.

1075



1076

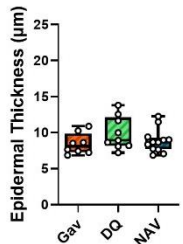
1077

1078 **Figure 1 – figure supplement 6. Functional and senescence markers in skeletal muscle after early**
1079 **intervention with D+Q or Navitoclax.** Muscle fibre cross-sectional area in oxidative (A) and non-
1080 oxidative (B) fibres from irradiated mice at 16 months of age. Frequencies of p21-positive myonuclei
1081 in oxidative (C) and glycolytic (D) fibres. E) TAF frequencies in myonuclei. Data are from at least 5
1082 animals/group.

1083

1084

1085



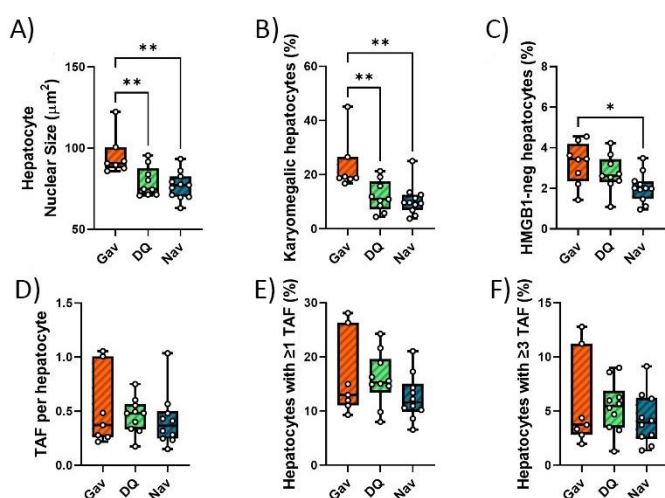
1086

1087

1088 **Figure 2 – Figure supplement 1. Late intervention with either D+Q or Navitoclax (at 12 months of**
1089 **age) does not change epithelial thickness at 16 months. Data are from at least 7 animals/group.**

1090

1091



1092

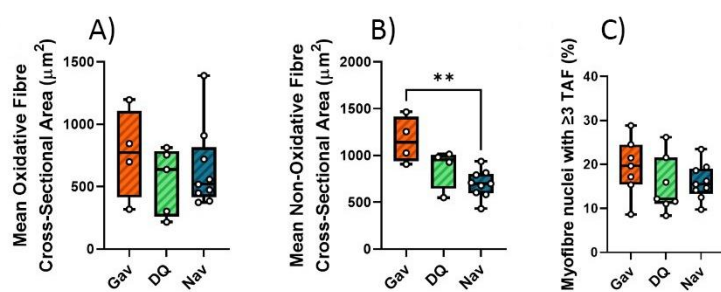
1093

1094 **Figure 2-figure supplement 2. Impact of late senolytics treatment on senescence markers in liver.**
1095 Nuclear size (A), percentage of karyomegalic hepatocytes (B), percentage of HMGB1-negative
1096 hepatocytes (C), TAF frequency per nucleus (D), frequency of TAF-positive cells (E) and frequency of
1097 cells with at least 3 TAF (F) in mice livers at 16 months of age, irradiated at 5 months and treated
1098 with either D+Q, Navitoclax or sham gavage at 12 months. Data are from at least 6 animals/group.

1099

1100

1101

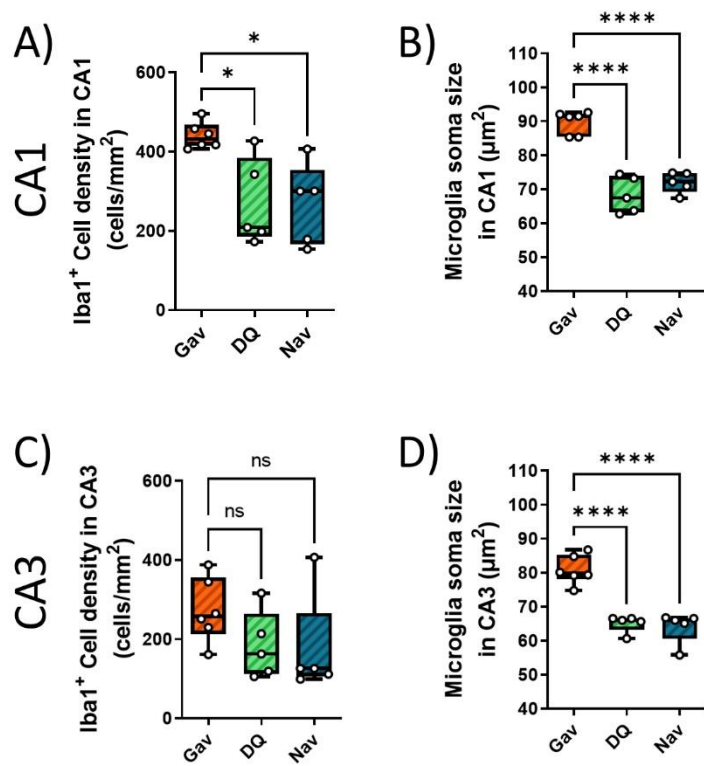


1102

1103

1104 **Figure 2-figure supplement 3. Functional and senescence markers in skeletal muscle after late**
1105 **intervention with D+Q or Navitoclax.** Muscle fibre cross-sectional area in oxidative (A) and non-
1106 oxidative (B) fibres from irradiated mice after late intervention at 16 months of age. C) TAF
1107 frequencies in myonuclei at 16 months of age after late senolytic intervention. Data are from at least
1108 5 animals/group.

1109



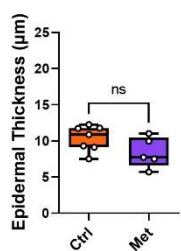
1110

1111 **Figure 2-figure supplement 4. Impact of late intervention on neuroinflammation.** Iba1⁺ cell density
1112 in CA1 (A) and CA3 (C). Iba1⁺ cell soma size in CA1 (B) and CA3 (D). Data are from at 5 -6
1113 animals/group.

1114

1115

1116



1117

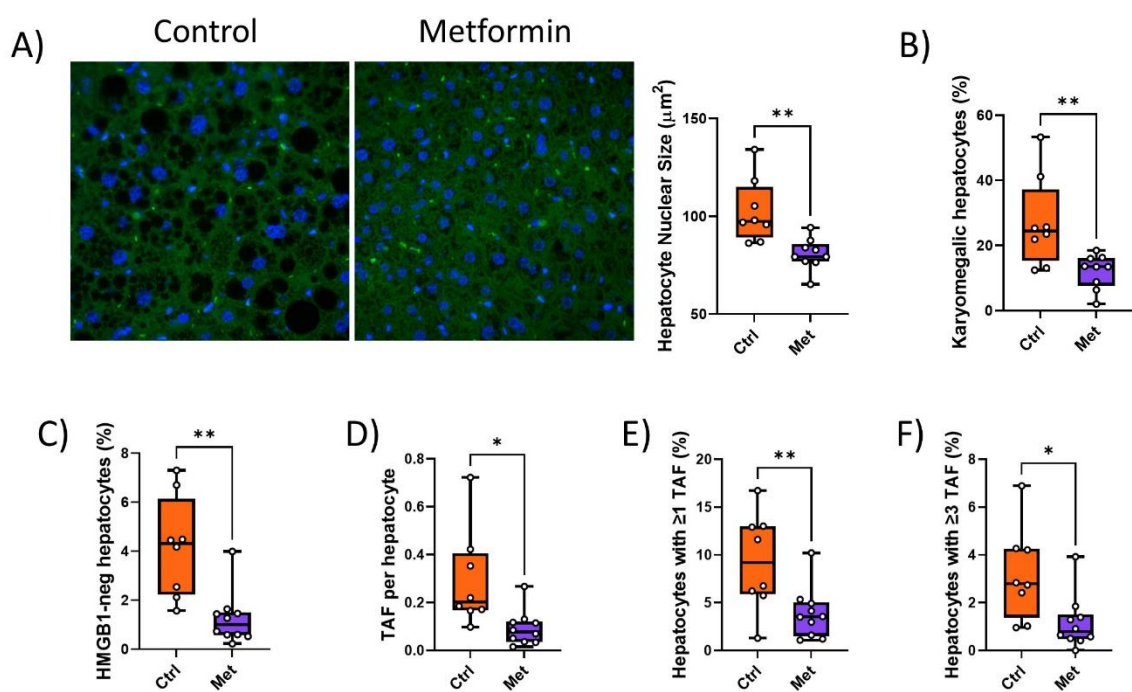
1118

1119 **Figure 3 – Figure supplement 1. Treatment of irradiated mice for 2.5 months with metformin**
1120 **(starting at 7 months of age) tends to reduce epidermal thickness at late age (16 months).** Data are
1121 from at least 6 animals/group.

1122

1123

1124

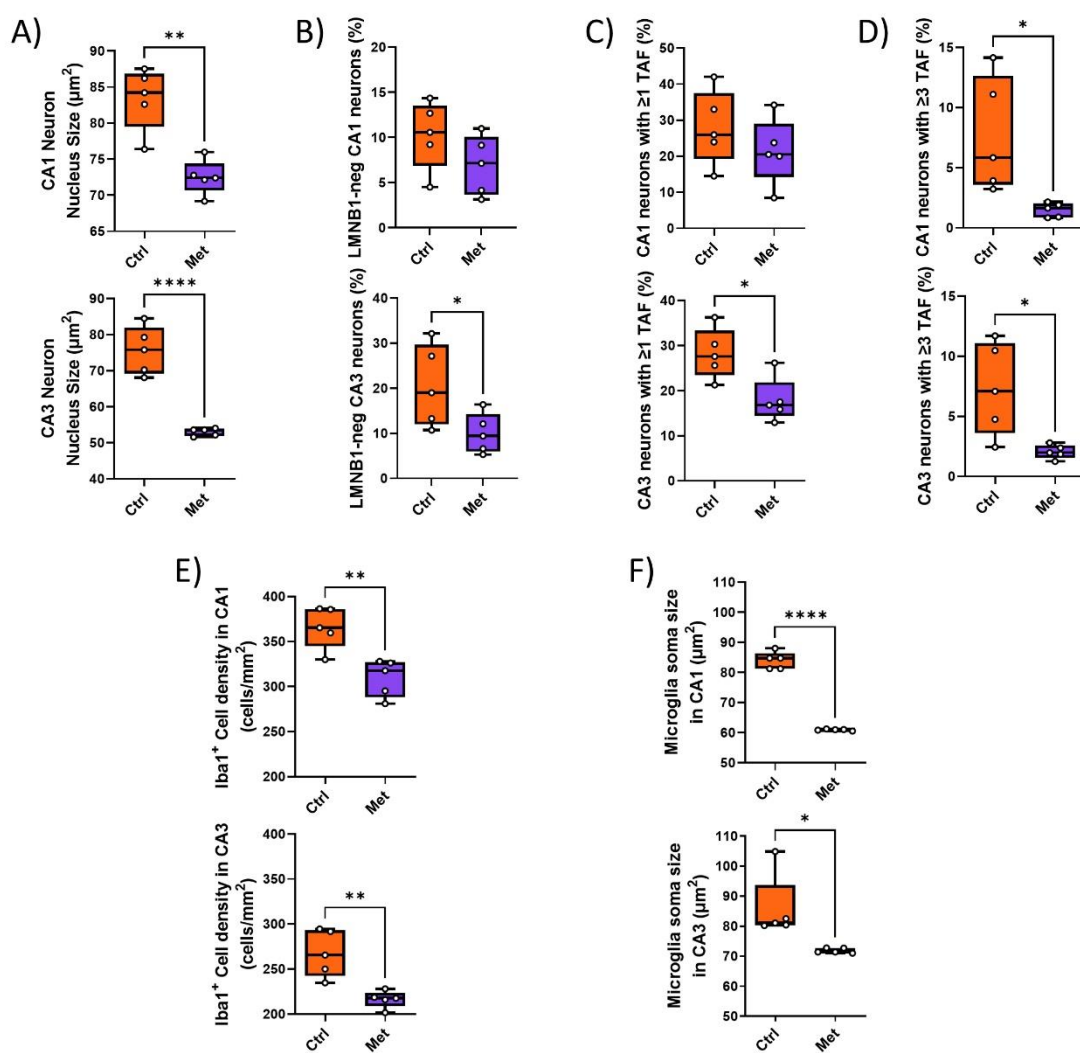


1125

1126

1127 **Figure 3 – Figure supplement 2. Impact of metformin on senescence markers in liver.** Mice were
1128 irradiated at 5 months of age and treated with metformin for 10 weeks starting at 6 months of age.
1129 A) Nuclear size with representative images (left, blue DAPI, green autofluorescence) and
1130 quantification (right). B) Frequency of karyomegalic hepatocytes. C) Frequency of hepatocytes
1131 negative for nuclearHMGB1. D) TAF frequency per nucleus. E) Frequency of hepatocytes with at least
1132 one TAF. F) Frequency of hepatocytes with at least 3 TAF. Data are from at least 6 animals per group
1133 at 16 months of age.

1134



1135

1136 **Figure 3 – Figure supplement 3. Senescence and neuroinflammation markers in hippocampus**
1137 **after intervention with metformin.** A) Neuron nuclear area in CA1 (top) and CA3 (bottom). B)

1138 Frequencies of laminB1-negative neurons in CA1 (top) and CA3 (bottom). C) Frequencies of TAF-

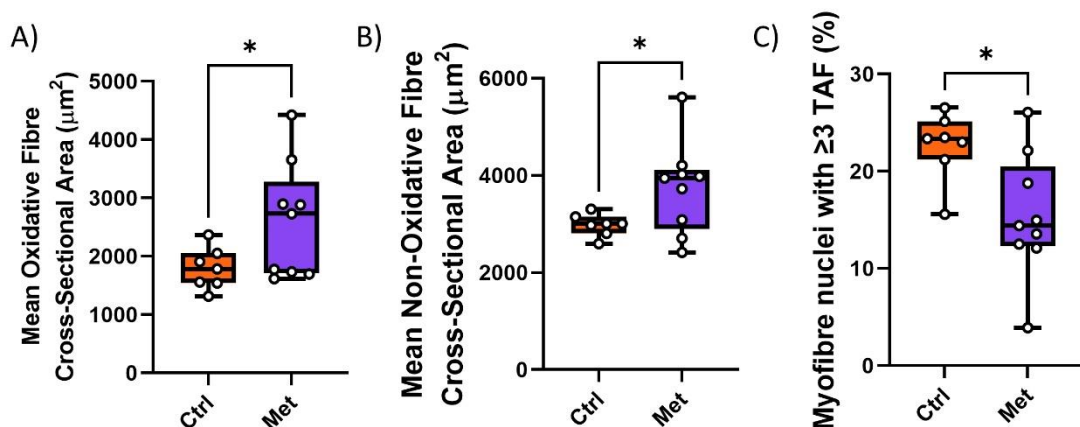
1139 positive neurons in CA1 (top) and CA3 (bottom). D) Frequencies of neurons with at least 3 TAF in CA1

1140 (top) and CA3 (bottom). E) Iba1⁺ cell density in CA1 (top) and CA3 (bottom). F) Iba1⁺ cell soma size in

1141 CA1 (top) and CA3 (bottom). Data are from at 5 -6 animals/group.

1142

1143



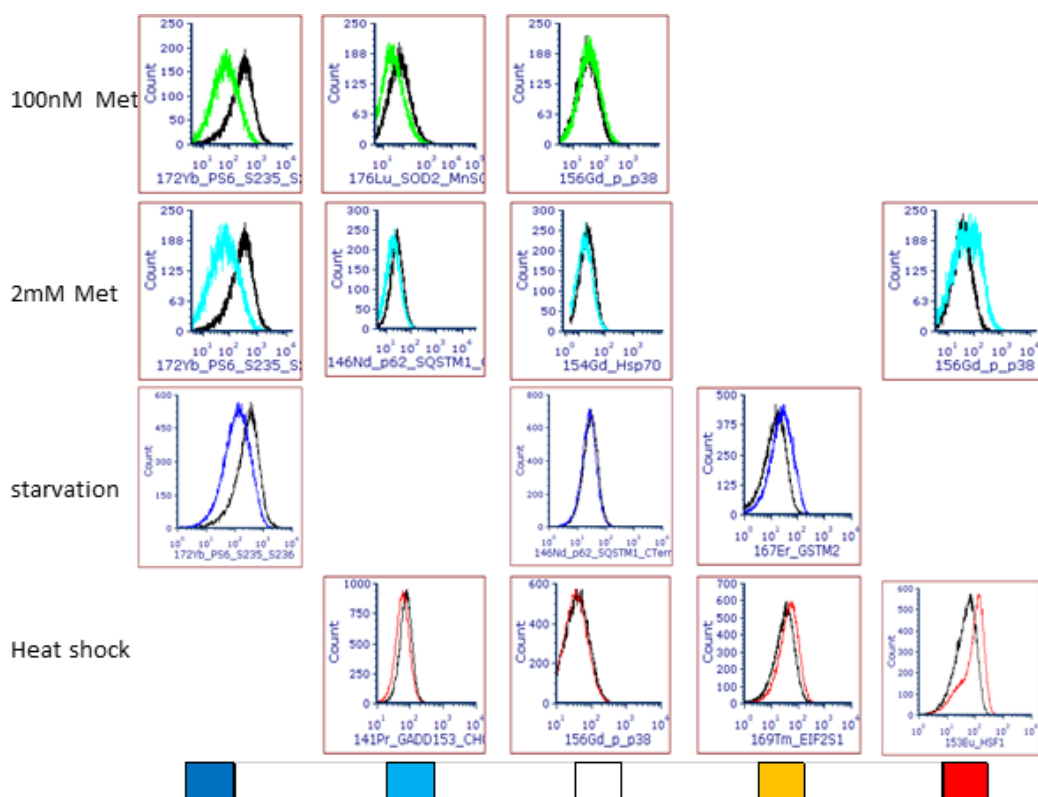
1144

1145

1146 **Figure 3 – Figure supplement 4. Impact of metformin on hind limb muscle.** Myofibre cross-
1147 sectional area of oxidative (A) and non-oxidative (B) fibres. C) Frequencies of TAF-positive myonuclei.
1148 Data are from at least 8 animals per group at 16 months of age

1149

1150



1151

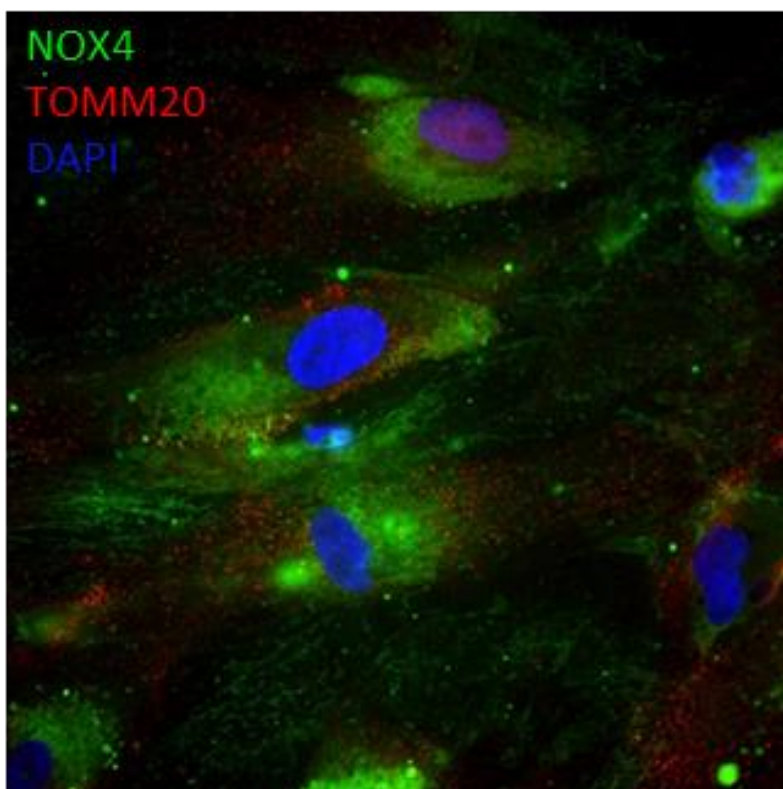
1152 **Figure 5 – Figure supplement 1. Representative histogram overlay examples for use of CyTOF as**
1153 **stress pathway identifier.** Treatments are indicated on the left. Colour codes at the bottom

1154 represent strong decrease (dark blue), mild decrease (light blue), no change (white), light increase

1155 (amber) or strong increase (red) and correspond to the heatmap in Fig. 5A.

1156

1157



1158

1159

1160 **Figure 6 – supplement 1. NOX4 does not co-localise with mitochondria.** Senescent MRC5
1161 fibroblasts, representative double staining with Nox4 (green) and TOMM20 (red). Blue: DAPI.